Microstructure and cyclic oxidation behavior of APS TBC systems drilled with various laser

methods

V. Ebrahimzade^{a,1}, H. Uchtmann^b, L. Singheiser^a, M. Krüger^a, J. Malzbender^a,

^aForschungszentrum Jülich GmbH, Microstructure and Properties of Materials (IEK-2), Institute

of Energy and Climate Research, 52425 Jülich, Germany

^bRWTH Aachen University, Chair for Laser Technology, Steinbachstrasse 15, 52074 Aachen,

Germany

Abstract

Aiming towards an optimization of drilling of cooling holes for gas turbine applications, thermal

barrier coated specimens were drilled with different laser set-ups. The investigated TBC system

consists of an APS deposited TBC, a MCrAlY bond coating (BC), and a Nickel-based super alloy.

The microstructural analysis was performed after laser drilling and also cyclic oxidation tests, in

order to understand the influence of different laser drilling parameters, i.e. trepanation/percussion

drilling, long-pulsed and ultra-short pulsed lasers, hole angle. Aiming towards this, the first test

series consisted of an assessment of specimens that were laser drilled with different parameters

and only analyzed regarding microstructural aspects, whereas the second series was based on

specimens that were laser drilled with various laser parameters and subsequently tested by cyclic

oxidization experiments. Initiation and progress of delamination as function of the number of

cycles was assessed from thermography images and correlated with complementary finite

element analysis.

Keywords: Thermal barrier coating; cooling holes; laser drilling; cyclic oxidation, microstructure,

nickel-based superalloy

1. Introduction

In order to provide a stable energy supply, especially in the near future when renewable energy resources with their related fluctuations are to be considered as the main commodity, stationary gas turbines remain a necessity. Gas turbines are advantageous since they are able to compensate fluctuations due to their relatively short start-up time and high load capability [1].

Advanced gas turbine blades are coated usually with M(=Ni, Co)CrAlY bond coatings (BC) [2] and ceramic thermal barrier coatings (TBCs) [3] and are typically perforated with a large number of cooling holes leading to an additional cooling effect by the virtue of film cooling of the TBC surface, thereby protecting the base material from the very high gas temperature up to 1500°C [4]. Currently cooling holes in rotating blades are typically drilled by electro-chemical machining (ECM) or electro-discharge machining (EDM) before application of the TBC, as well as recently by laser drilling, after application of TBC [5]. However, due to time and cost issues laser drilling of cooling holes receives growing interest in the last years [6].

Currently, the main problem using laser drilling techniques appears to be the limited quality of cooling holes, which makes them a critical life limiting factor [7]. The limited quality of such holes is mainly related to the material removal process by long-pulsed laser drilling, which is melting-dominated [6, 8, 9] and induces defects such as geometrical imperfections, recast layers, oxide layers, heat affected zone (HAZ), and cracks at interfaces and/or grain boundaries of the substrate [9]. The defect density can be affected by different laser parameters such as peak power, assist gas, pulse frequency, hole angle, trepanation/percussion drilling mode etc. [10-12].

Trepanation drilling, i.e. laser drilling with a circular movement of the laser beam similar to a cutting process, has been suggested in literature [13-15] as a method to provide better quality holes compared to percussion drilling, i.e. laser drilling with a fixed laser beam of a larger diameter compared with trepanation, see Figure 1. Trepanation can also be used to drill larger

holes with good quality, as it is more similar to a conventional cutting process. However, a detailed comparison of these two drilling modes appears not to be available in literature, which is hence one of the focus points of this study.

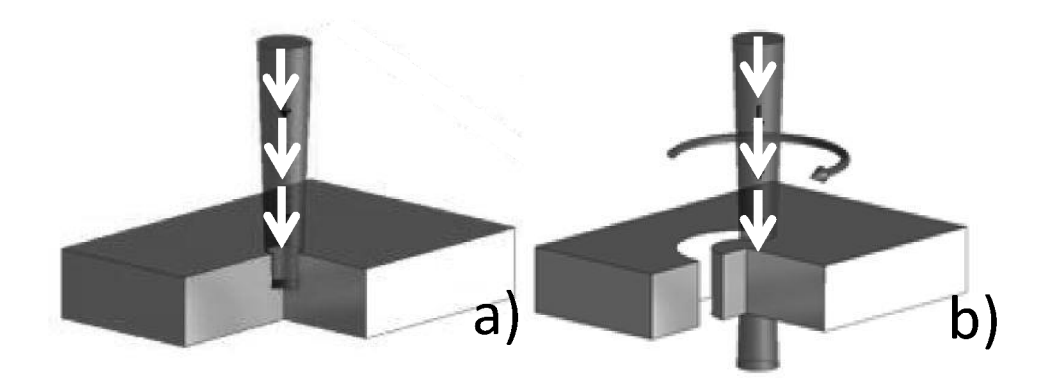


Figure 1a) Percussion and b) trepanation drilling.

Several studies have aimed towards an understanding of the influence of the angle on the quality of laser-drilled holes. It was reported by Sezer et al. [8] that in the case of inclined holes delamination of TBC seems to be more critical than for vertical holes. Associated cracks could lead to premature TBC delamination, severe oxidation of BC or substrate and deterioration of mechanical properties of the TBC system. Kamalu et al. [16] explained the initiation and propagation of such delamination cracks as a 2-step process. It was proposed that crack initiation occurs already after the first laser pulse due to thermal stresses induced by thermal mismatches of different components in TBC system. Crack propagation is caused then by the recoil pressure during the subsequent pulses, as well as mechanical stresses associated with the ejection of melt. Sezer et al. [9] suggested, based on a CFD analysis, that, since the melting is ejected with a higher velocity at the leading edge compared with trailing edge (see Figure 14 in results section for definition), higher normal and shear mechanical forces are exerted on the hole wall at this area, thereby increasing the probability of coating delamination and corrosion. They also showed the influence of the angle of drilling on the defects at the cooling hole, where higher inclination increased the thickness of recast, oxide and HAZ layer. TBC delamination were also increased

with the decreasing of the hole angle with respect to the TBC surface. Girardot et al. [17] made an effort to quantify the influence of angle on damaging factors. Using numerical calculations, they showed that forces are larger in case of inclined holes, independent of TBC thickness. However, the moment, due to the recoil pressure, at interfaces near the hole is higher for thicker coatings.

Very few studies concentrated on the behavior of laser drilled TBC systems under thermal cycling conditions [18-20]. Das et al. [20] investigated drilling of round cooling holes with an ultra-short pulsed laser, featuring a pulse width in range of femtoseconds, for a wall thickness of 1.5 mm. As expected for this advanced method, they could not find severe defects or recast layers on the hole wall. Furthermore, no localized delamination cracks were found at the hole after thermal cycling. Lugscheider et al. [18] tested two types of drilled TBC systems. Type one was drilled after the coating of the substrate. For type two, the substrate with BC was drilled and then coated with TBC, resulting in fewer defects at the interfaces. The lifetime of the type two specimens after thermal cycling was much longer than that of type one. Nonetheless, thermal cycling of laser drilled TBC systems as well as the delamination behavior of the coating near the holes has not been in focus so far, which is hence analyzed in this work.

In the current work, a detailed analysis of the influence of different laser drilling modes and hole angles as well as cyclic oxidation on the microstructure of the samples is presented. In order to understand the development of delamination cracks during the tests, thermography measurements after intervals of few cycles were also performed. To improve the understanding of the experimental observations, regarding the influence of hole angle during thermal cycling, complementary FEM simulations were performed. After failure and preparation of cross-sections, the microstructure, especially at the hole, has been analyzed using scanning electron microscopy (SEM), electron backscatter diffraction (EBSD) for orientation mapping, and energy-dispersive spectroscopy (EDS) for characterizing of the elemental composition.

2. Experimental

Specimens' choice for each test series and number of tests was limited by materials availability.

Hence series one and series two were based on different TBC systems concentrating on different aspects that could be investigated independently.

2.1 Laser drilling of TBC systems

Within the framework of the first series, flat specimens were laser drilled with fiber and flash lamp laser, including trepanation and percussion drilling modes at different drilling angles (90° and 30°), as well as ultra-short pulsed laser, see Table 1. The base material was a nickel-based superalloy (3 mm), PWA 1483, the BC Sicoat 2464 (180-300 μ m), and APS TBC was deposited from an IKH powder with a porosity of 18+/-4% (500 μ m). The nominal diameter of all the holes was 0.5 mm. The laser parameters used for drilling are listed in Table 2. These parameters were based on results obtained within the framework of projects carried out at the chair of laser technology (LLT) at RWTH Aachen university.

Table 1 Test matrix for laser drilled TBC systems, series one.

Specimen type	hole diameter (mm)	Angle
Fiber laser, percussion	0.5	90
	0.5	30
Fiber laser, trepanation	0.5	90
	0.5	30
Flash lamp, percussion	0.5	90
	0.5	30
Ultra-short pulsed laser	0.5	90

Table 2 Laser parameters used for drilling the specimens.

Laser parameter	Flash, perc.,	Fiber, trep.,	Fiber, perc.,	Ultra-short pulsed laser,
Power, kW	90° & 30° 7.3	90° & 30° 5.5	90° & 30° 6	90° 80·10 ⁻³
Pulse width, ms	0.75	0.5	0.7	-
Repetition rate, Hz	20	100	60	$238 \cdot 10^3$
Process gas /		coı	mpressed air / 5	
pressure, bar				

2.2 Cyclic oxidation of laser drilled TBC systems

Cyclic oxidation tests were performed in order to understand the effect of different laser drilling parameters for a TBC system with and without cooling holes on TBC system life time and TBC spallation. Within the framework of the test series two, the TBC system is considered to be a model material and it is based on a nickel-based superalloy, IN792, $(0.7 \pm 0.3 \text{mm})$ with two types of bond coat $(200 \, \mu\text{m})$: aluminized LCO22 and not aluminized PWA286, and an air-plasma sprayed TBC coating $(300 \, \mu\text{m})$, see Table 3. The TBC coating consists of yttrium-stabilized zirconia with the percentage ratio $92 \, \% \, / \, 8 \, \% \, (Y_2O_3/ZrO_2)$.

Table 3 Specimen types for cyclic oxidation tests.

Substrate	In792 CC/ 0.7±0.3 mm		
ВС	LCO22 / 200 μm	PWA 286 / 200 μm	
TBC	aluminized APS	/ 300 µm	
Specimens length	ca. 18 mm		
Number	6	4	

To study the influence of the hole angle on the behavior of the TBC system, the cooling holes were drilled using flash lamp laser (laser device: LASAG FLS 652 N) with percussion mode at 90° (200 pulses) and 30° (400 pulses) degree with respect to the surface of TBC. The cooling holes were also drilled with fiber laser (laser device: IPG YLS-600/6000-QCW-AC), using percussion mode and trepanation mode. The test matrix is shown in Table 4. The hole diameter was in all cases 0.5 mm. The specimens had a cylindrical geometry with three rows of holes with 120° shift, at each row two holes, see Figure 2.

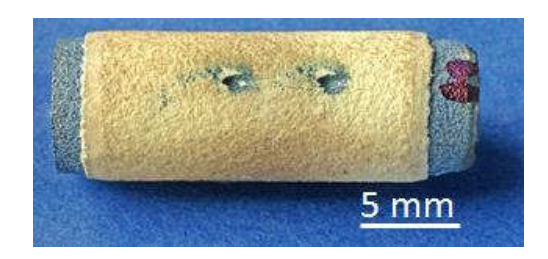


Figure 2 A cyclic-oxidation-specimen with laser drilled holes.

Table 4 Test matrix for cyclic oxidation tests.

		Bond Co	oat Type		
Drilling method	LCO22		PWA 286		
Drining mounds	Hole Diameter, Angle mm		Hole Diameter,	Angle	
Undrilled	Yes		no specimen available		
Flash lamp,	0.5	90	0.5	90	
Percussion	0.5	30	0.5	30	
Fiber, Trepanation	0.5	30	0.5	30	
Fiber, Percussion	0.5	30	0.5	30	

Cyclic oxidation tests were performed using a tube furnace (Carbolite-Gero GmbH, Model 301), with a minimum temperature of 100°C and a maximum of 1050°C, a heating time of 12 min, a

hold time of 2 hours at the maximum temperature, see Figure 3, as well as a cooling time of 5 min. Failure was defined as the number of cycles till when a macro-crack could be observed by visual inspection.

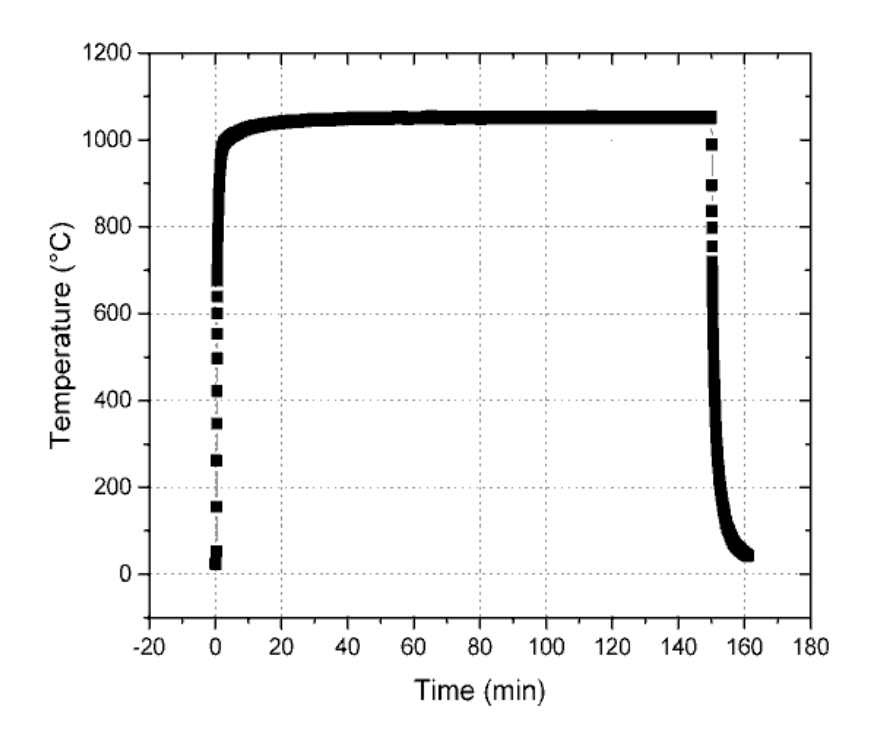


Figure 3 Measured specimen's temperature in the cyclic oxidation oven.

Within selected time intervals, thermography images were recorded using an infrared camera (FLIR, ThermaCam SC3000). For thermography images, the samples were heated in 0.4 s using two flash lamps. During cooling-down, 20 images were recorded with a frequency of 50 Hz. The images were obtained using the temperature profile analysis module available by the software ThermoLab [21]. At positions, where the coating was delaminated, the heat flux into the base material decreases leading locally to a higher temperature compared with the surroundings. As for "Greenish" thermography images given in the results section, green areas represent areas with the interface in-contact, and yellow to red areas represent delaminated regions.

Before metallographical examinations, specimens were embedded in a mixture of epoxy and hardener solution. After hardening of the epoxy, specimens were cut at the laser holes using ISOMET 400 cutting machine from Buehler. Afterwards, specimens were grinded and then polished with suspensions with 6, 3 and 1 µm sized diamond particles.

After the necessary preparation of the specimens, microstructural analysis was performed using secondary electron microscopy (SEM), using a Zeiss SUPRA 50 VP, electron backscattered diffraction (EBSD) using the machine Oxford Instruments X-Max, and energy dispersive spectroscopy (EDS) by Oxford Instruments Nordlys.

2.3 FEM Modelling of stress evolution during a thermal cycle

In order to analyze more precisely the influence of the angle on the stress distribution at the hole, a 3D model was created for FEM analysis using the software Abaqus. 10-node quadratic tetrahedral elements, C3D10, were used in the analysis. In order to save computational time for the model with vertical and inclined hole, two and three symmetry surfaces have been defined respectively, as shown in Figure 4. The TGO thickness was also assumed to be negligible in the 3D model to reduce computation time.

Figure 4 shows the 3D models of the TBC system including vertical and inclined holes. As for vertical hole, SS1 is the cyclic symmetry surface, i.e. simulating the hole as a part of a cylinder, whereas SS2 and SS3 are the symmetry surfaces with respect to 1-3 (r-z) and 1-2 (r- θ) planes, respectively, see Figure 4a. For an inclined hole, symmetry surface SS1 (opposite side of the hole) is defined to simulate the cyclic symmetry as well. To implement cyclic symmetry, degree of freedom in tangential direction 2 (θ) was constrained. SS2 is the symmetry surface (at hole) with respect to 1-3 (r-z) plane in cylindrical coordinate system, see Figure 4b. For SS2, the degree of freedom was constrained in the normal direction of the plane.

Additionally, Figure 4 shows the paths where the stress distributions for vertical and inclined (30°) holes will be compared; the red path is in the TBC layer at the TBC/BC interface. With respect to the loading, a homogenous temperature distribution was assigned to every node, reducing from 1050° C to 100° C over 211 s. A free stress state was assumed at the beginning of thermal loading due to enough stress relaxation after enough high temperature exposure. The hole diameter, TBC, BC, and substrate thickness in the FEM model were 0.5 mm, 500 μ m, 250 μ m, and 1.75 mm, respectively. In the FEM model, different range of thicknesses, compared with the tested materials, were chosen. However, a thinner substrate, in regard with the tested specimens in section 2.2 Cyclic oxidation of laser drilled TBC systems, leads to more critical situation than a thicker substrate [22].

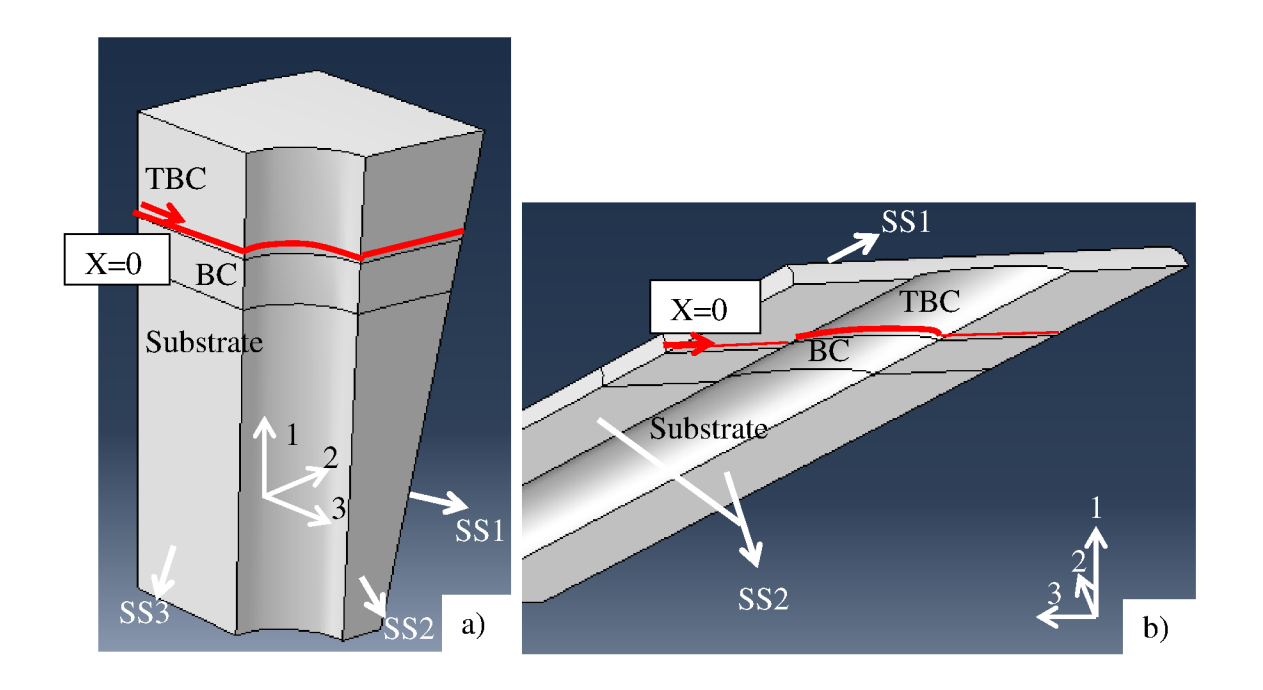


Figure 4 The red path TBC/BC interface over which the stress distributions are shown for (a) vertical and (b) inclined cooling hole.

3. Results and Discussion

3.1 Investigation of Laser drilled TBC systems using SEM

In the following microstructural analysis of flat laser drilled specimens of series one, see Table 1 and section 2.1 Laser drilling of TBC systems, drilled with different laser methods are presented. Cross-sections of the specimens having vertical and inclined holes drilled with fiber laser, in both percussion and trepanation mode, provide useful information about typical imperfections and defects at such holes. Typical defects resulting from laser drilling are i) deviation of cooling hole diameter, ii) cracking between TBC and BC or BC and substrate, iii) cracks at substrate grain boundaries, iiii) recast layer as a consequence of insufficient removal of melt during laser processing, see Figure 5 and Figure 6. For both percussion and trepanation drilling with fiber laser, inclined holes showed longer cracks, see the trepanated specimens in Figure 5a-b. The crack length measurement results of all specimens are summarized in Table 5. Comparing percussion and trepanation drilling, it can be derived that a better hole quality, with shorter crack lengths, can be achieved using trepanation drilling.

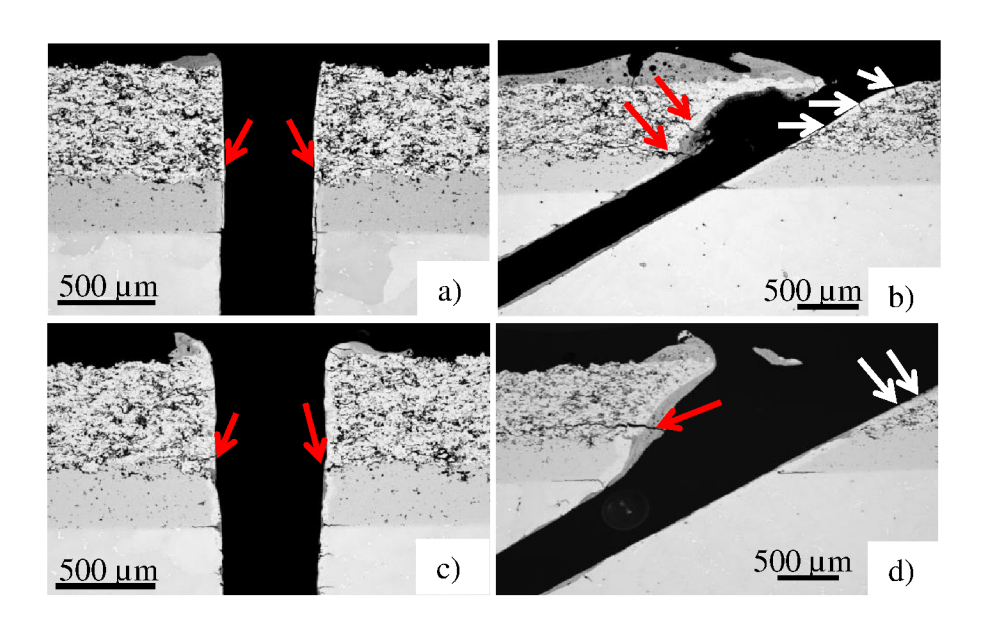


Figure 5 SEM images of specimens drilled with fiber laser using trepanation mode for a) 90° and b) 30° holes, and percussion mode similarly for a c) 90° and d) 30° holes. Arrows in red show cracks at TBC/BC interface, and arrows in white indicate cracks in TBC recast layer.

Typical microstructural defects of the specimen drilled with long-pulsed laser sources are shown in Figure 6, where a TBC recast layer with negligible pore density as well as the BC/substrate recast layer, including oxide particles, can be observed in Figure 6b and c.

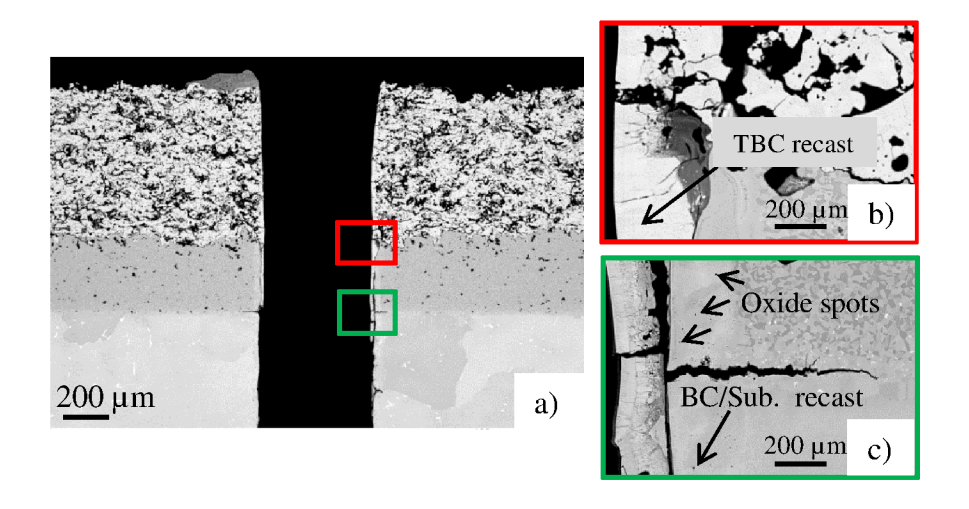


Figure 6 a) A TBC system drilled by a ms-pulsed laser with b) TBC and c) substrate/BC recast layer.

Figure 7 presents the SEM images of the specimen drilled with ultra-short pulsed laser. It can be observed that the density of the defects at the hole is negligible in comparison with other laser methods. However, the parameter set is still not fully optimized, as imperfections in the TBC layer can be observed.

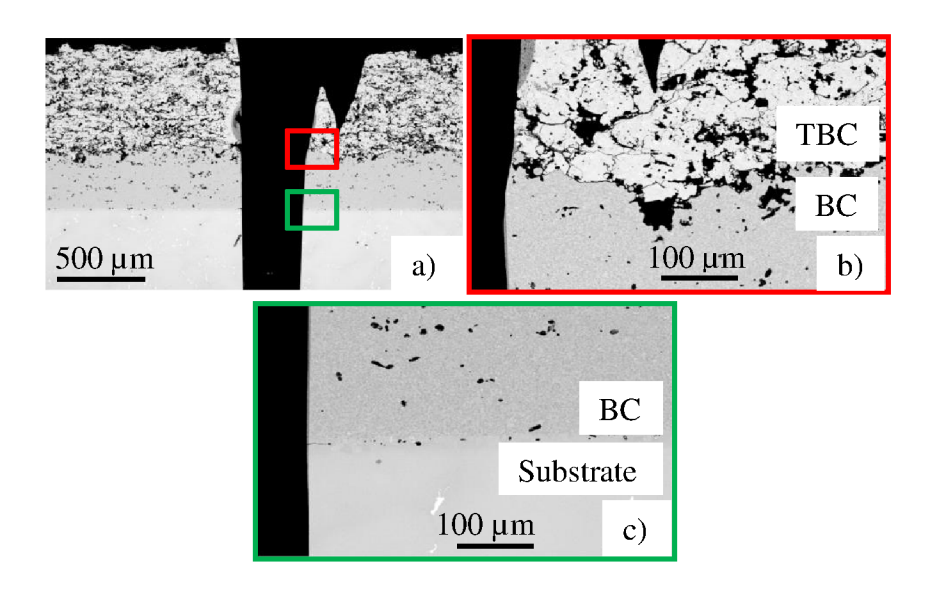


Figure 7 SEM images of specimens drilled with a) ultra-short pulsed laser, and magnified image b) at TBC/BC interface, and c) at BC/substrate image.

In the following, crack lengths for specimens drilled with fiber laser, percussion and trepanation mode, flash lamp, percussion, as well as ultra-short pulsed laser, are presented, see in Table 5. For the measurements of these parameters the software AnalySIS Pro has been used. It can be observed that cracks are longer in case of percussion drilling in comparison with the trepanation mode, as also reported in literature [13]. This is likely to be related to the lower pulse energy of 2.7 J in the trepanation mode, compared to 4.2 J in the percussion mode [14, 15]. The analyzed cross-section of the inclined hole drilled with fiber laser trepanation is slightly off the middle section of the hole, however, considering with vertical holes, a similar trend has been observed. Moreover, ultra-short pulsed laser drilling demonstrates better quality with a negligible defect density, which is due to very short pulse width. It has been reported in literature that in case of laser drilling with pulse widths in the range of femtoseconds the material vaporizes, i.e. no recast layer is observed on the hole wall. Dou et al. [23] showed that the material needs at least pulses in the range of 1.5-3 picoseconds so that heat can transmitted through electrons and the lattice. Therefore, it is not possible for heat to be conducted from the laser pulse to the adjacent regions, i.e. no HAZ has been observed [24].

It can be concluded on the basis of several studies in literature that the cracking behavior [9, 16, 25, 26] is due a result of the combination of several mechanisms; suggested are solidification cracking, liquation cracking, melt ejection process etc. Solidification cracking occurs due to the cooling after laser drilling process, where thermal stress especially at the interfaces can cause crack initiation [25]. Liquation cracking is induced by melting of second phase particles (NbC for example) in HAZ at grain boundaries of the superalloy at sub-solidus or super-solidus temperature, which leads to intergranular, hot cracking [26]. This happens due to formation of eutectics between the constituent of the second phase particle (Nb in this example) and the surrounding matrix (Ni in case of a nickel-based superalloy), which results in an eutectic phase with a lower melting point leading to crack initiation at high temperatures. The melt ejection

process leads also to stresses to the hole wall, which also appear to play a role in the crack initiation process [9, 16].

It is also clear from this table that larger defects occur for inclined holes. Additionally, in case of percussion drilling, fiber laser, probably due to larger pulse frequency, 60 Hz, compared with flash lamp laser, 20 Hz, more defects at the hole are induced at the TBC/BC as well as BC/substrate interfaces, as also reported by Sezer et al. [27]. However, they observed with increasing pulse frequency a decrease in the number of delamination cracks at BC/substrate interface, which is not the case in our observations. The upward melt ejection, and TBC undercutting at TBC/BC interface (especially for inclined holes), see Figure 8, increased with increasing pulse frequency, which is due to increased TBC wall temperature. The melt ejection process, TBC undercutting, as well as the eroded region on the leading edge, induces higher mechanical stress and moment at the TBC/BC interface initiating or propagating the delamination crack [27]. The thicker recast layer with increasing pulse frequency results also to larger solidification cracking especially at BC/substrate interface, [11]. For the case of flash lamp percussion, inclined drilling, the analyzed cross-section is slightly off the middle section of the hole. However, in comparison with fiber laser percussion drilling, the same trend is observed as for vertical holes.

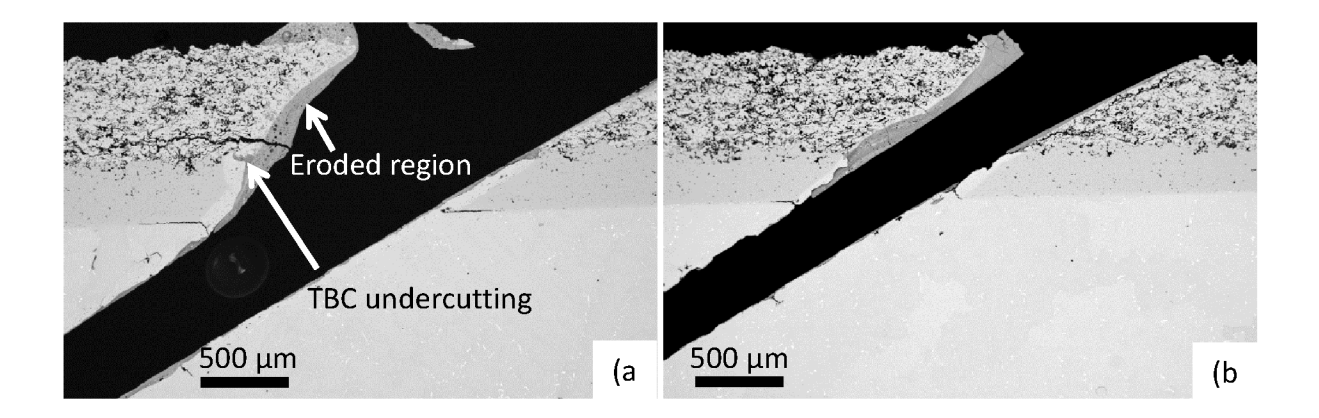


Figure 8 The TBC undercutting observed for the case of a) fiber laser, percussion, compared with b) flash lamp, percussion laser drilling.

Table 5 Measurement of averaged crack length in TBC layer, at BC/substrate interface (shown as BC/Sub int.), and in the substrate. trep: trepanation, perc: percussion.

Crack	Fiber,	Fiber,	Fiber,	Fiber,	Flash,	Flash,	UKP,
length, μm	trep., 90°	trep., 30°	perc., 90°	perc., 30°	perc, 90°	perc, 30°	90°
TBC	37 ± 31	103 ± 94	142 ± 70	337 ± 436	94 ± 74	100 ± 107	41 ± 33
BC/Sub int.	71 ± 15	138 ± 42	156 ± 7	400 ± 50	47 ± 22	136 ± 35	20 ± 10
Substrate	42 ± 9	52 ± 5	58 ± 22	91	78 ± 12	50 ± 26	0

The average thicknesses of the TBC recast and BC/substrate recast layers are analyzed using the same software. As shown in Table 6, percussion drilling of vertical holes (by fiber laser) results in thicker recast layers at TBC as well as at BC and substrate near the hole, than in the case of trepanation drilling. This is likely to be due to the fact that the higher pulse intensity in case of trepanation (smaller laser beam radius) leads to an increase in melt ejection and possibly its vaporization, resulting in a thinner recast layer [12]. Moreover, using flash lamp laser with percussion mode caused a reduction especially in TBC recast layer thickness in comparison with fiber laser probably due to higher pulse frequency by the former laser method, as mentioned earlier. This can be due to the increase in laser average power as well as the shortening of the time between successive pulses so that the molten material can be removed before the start of the subsequent pulse [11]. Regarding inclined holes, a thicker recast layer than for vertical holes is also observed [9]. On the other hand, ultra-short pulsed laser offers the best quality with the thinnest recast layers.

Figure 9 shows SEM images of the BC/substrate interface for specimens drilled with different laser methods. One can obtain a better understanding of the measurements of recast thickness and crack length presented in Table 5 and Table 6.

Table 6 Measured averaged thickness of TBC and BC/substrate recast layers. trep.: trepanation, perc.: percussion.

Recast	Fiber,	Fiber,	Fiber,	Fiber,	Flash,	Flash,	UKP,
thickness	trep., 90°	trep., 30°	perc., 90°	perc., 30°	perc, 90°	perc, 30°	90°
TBC	19 ± 8	83 ± 46	56 ± 17	77 ± 24	35 ± 12	33 ± 12	33 ± 19
BC/Sub.	23 ± 7	28 ± 9	29 ± 15	45 ± 23	25± 16	50 ± 22	-

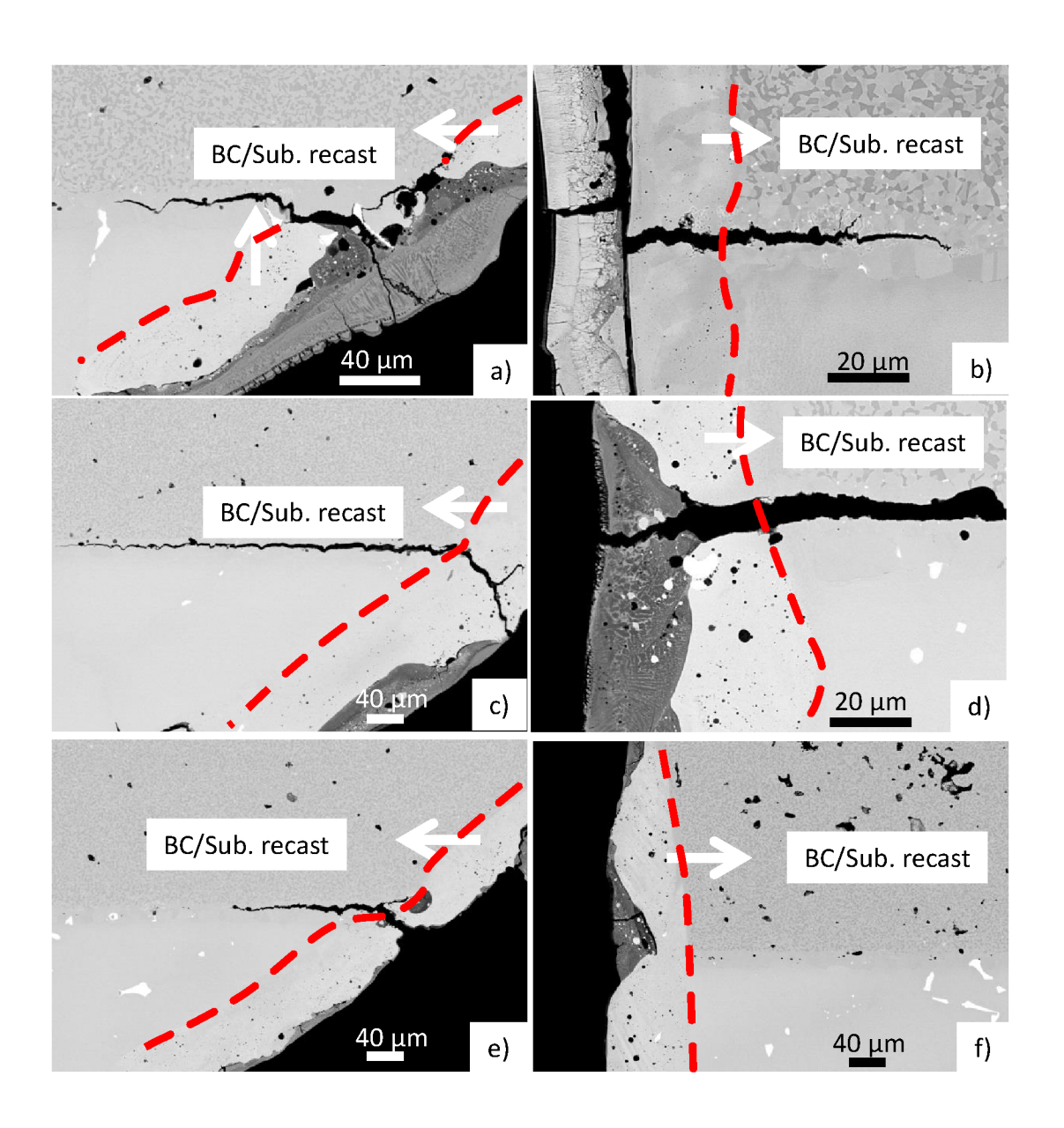


Figure 9 Comparison of BC/Sub. recast thickness and crack length for a) fiber laser, trep., 30° , b) fiber laser, trep., 90° , c) fiber laser, perc., 30° , d) fiber laser, perc., 90° , e) flash laser, perc., 30° , f) flash laser, perc., 90° .

3.2 Cyclic oxidation of drilled and undrilled TBC systems

In the following microstructural analysis of cylindrical specimens of series two, drilled with different laser methods and thermal cycled, are presented, see Table 4 and section

2.2 Cyclic oxidation of laser drilled TBC systems.

3.2.1 Thermography images and comparison with FEM results

It has been illustrated in literature [28, 29] that thermography is a useful method to examine the delamination of TBCs. Thermography experiments performed for specimens after different number of thermal cycles, from the beginning to failure, are shown and discussed in the following. In Figure 10, for instance, the formation and propagation of delaminations for two specimens (BC type: aluminized LCO22), for vertical and inclined holes drilled with flash lamp laser using percussion mode, are compared. It can be concluded from these images that the delamination cracks are more pronounced at the holes for inclined holes than for vertical holes. Although not shown in details, the thermography images of the remaining tested specimens, drilled with fiber laser using trepanation and percussion mode as well as the ones with PWA286 BC revealed rather similar trends.

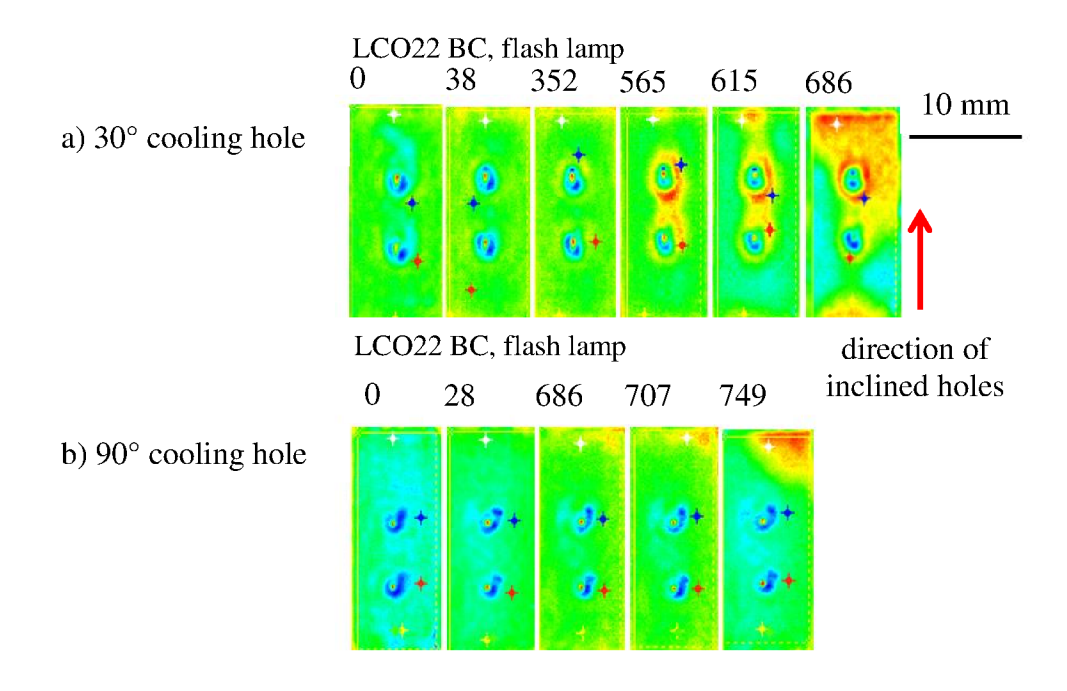


Figure 10 The development of delamination for specimens during cyclic oxidation test, drilled by flash lamp laser, with a) 30° and b) 90° cooling holes.

In Figure 11, the thermography measurements after laser drilling of inclined and vertical holes, before and after cycling, are shown. Contrary to 90° holes, delaminated regions at the 30° holes can be already recognized after drilling, indicated with red arrows.

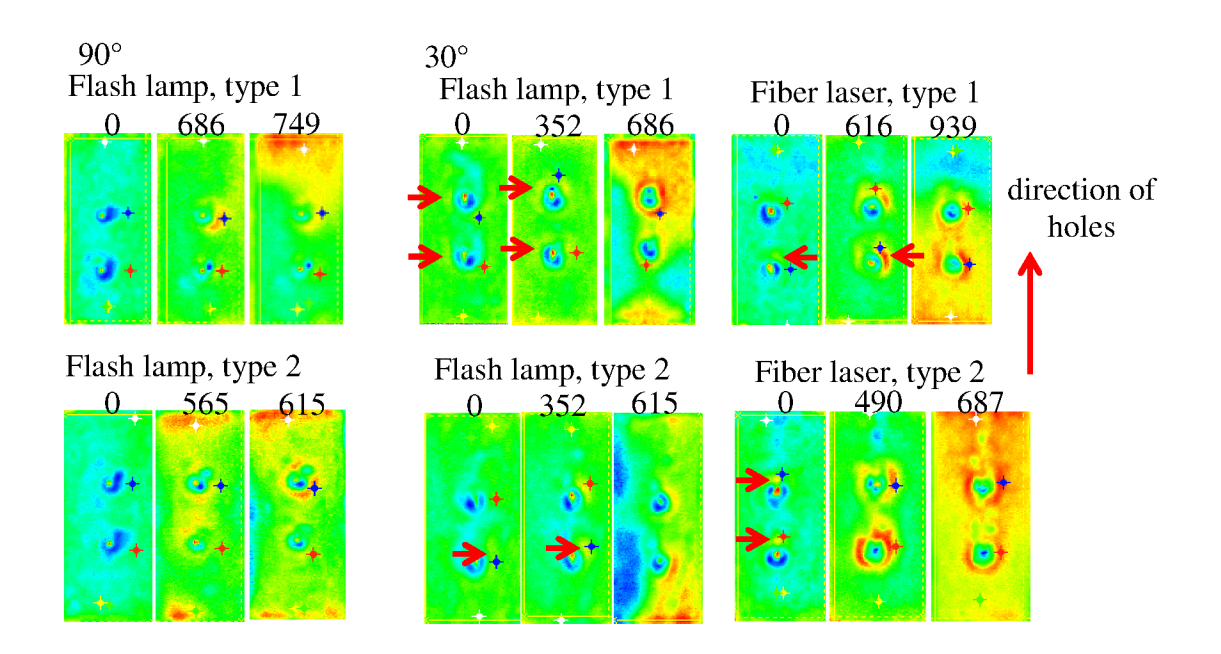


Figure 11 The development of delamination for the laser drilled specimen due to cyclic oxidation. Type 1: specimens with aluminized LCO22 as BC, and type 2: specimens with PWA286 BC. The delaminated regions mostly occur at the leading edge as well as at the sides of the hole, which reveals to be a critical crack initiation position for these inclined holes, which has not been reported in previous works. Figure 12 illustrates the critical position for crack initiation and propagation at the TBC/BC interface for an inclined hole.

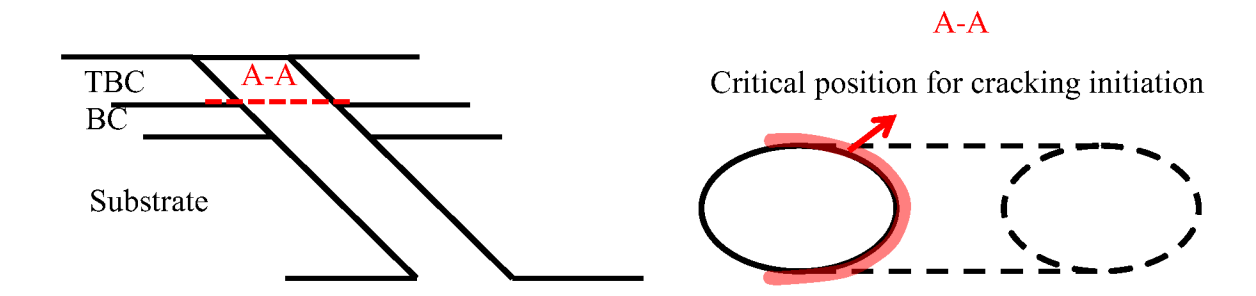


Figure 12 Schematic presentation of an inclined hole with the critical position at the TBC/BC interface for crack initiation and propagation under a cyclic oxidation loading condition.

In the following, the stress distributions for the two cases, vertical and inclined hole, are compared on the basis of 3D FEM models. Figure 13a and b reveal a difference in stress distribution for these two hole geometries. As can be seen, the stresses near the leading edge are higher for the inclined than for the vertical hole, which is in agreement with the experimentally observed failure behavior illustrated in Figure 11. Figure 13c shows the normal stress profile at TBC/BC interface (in TBC layer) over the red path highlighted in Figure 4. As can be seen, the largest normal stresses occur near the leading edge, in agreement with conclusions based on experimental results, see Figure 12.

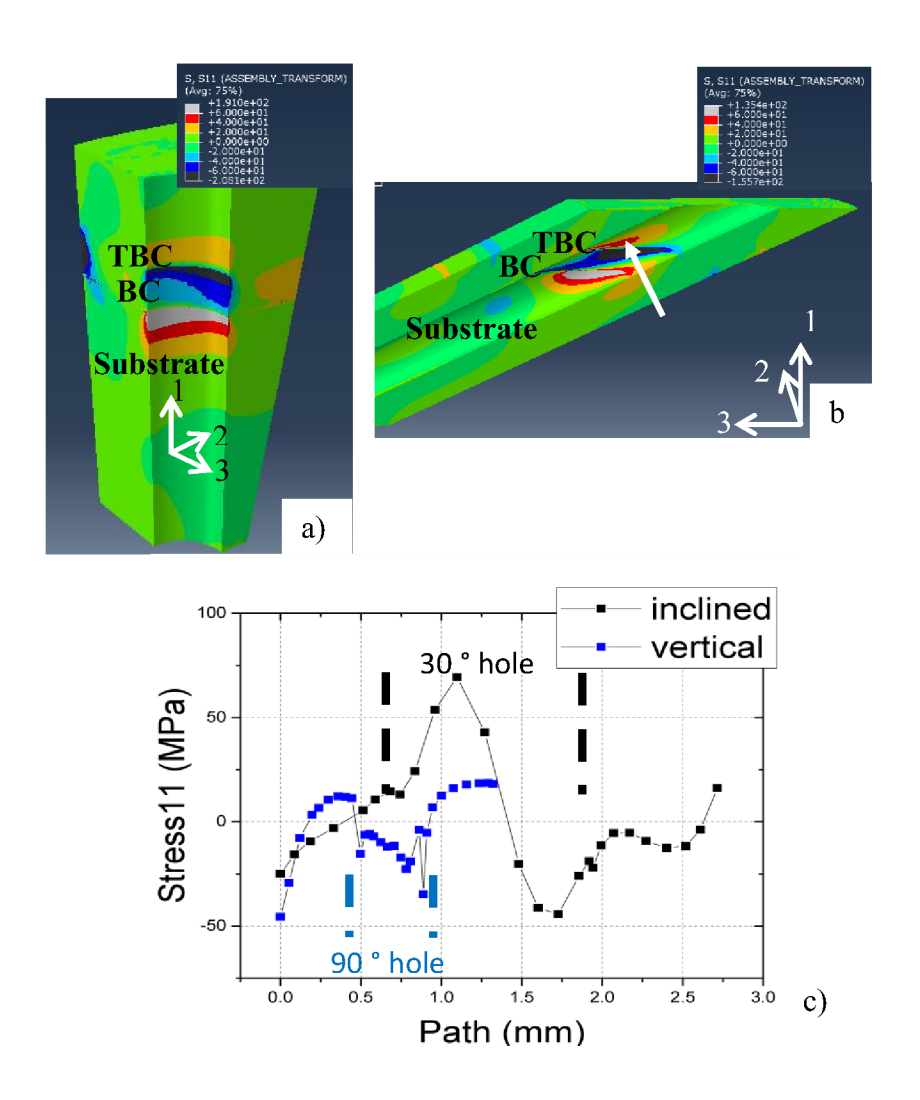


Figure 13 Stress distribution in the normal direction 1 at TBC/BC interface for a) vertical and b) inclined hole, c) normal stress profile at TBC/BC interface for both angles.

3.3 Microstructural analysis

In this section, microstructural analysis results of the specimen types with aluminized LCO22 BC in the as-drilled and tested case, drilled with fiber laser, trepanation mode, are presented and compared. Afterwards, the influence of the laser method, hole angle, and drilling mode, i.e. percussion and trepanation, on the damaging mechanisms during cyclic oxidation is discussed.

Microstructural images of the as-drilled specimen for the location near the hole are given in Figure 14. A large delamination crack can be observed at the leading edge after laser drilling. Several cracks formed that at the hole can be observed as well. Such cracks are formed mostly within recast layer at interfaces or substrate's grain boundary. Cyclic oxidation of the specimen can lead to further propagation and oxidation of these cracks in the BC and substrate, therefore, they must be avoided. The BC/substrate recast layer is composed of mainly γ (red) phase and has on average finer grains in comparison with the substrate grain size (see Figure 15). Since the grains of this layer are finer, its creep resistance at higher temperature decreases more than that of the substrate. The zirconia recast layer, shown in yellow in Figure 14b, is induced by TBC melting during laser drilling. There can be also an oxide layer on the hole wall which develops as a result of the high temperature exposure of the BC/substrate recast layer.

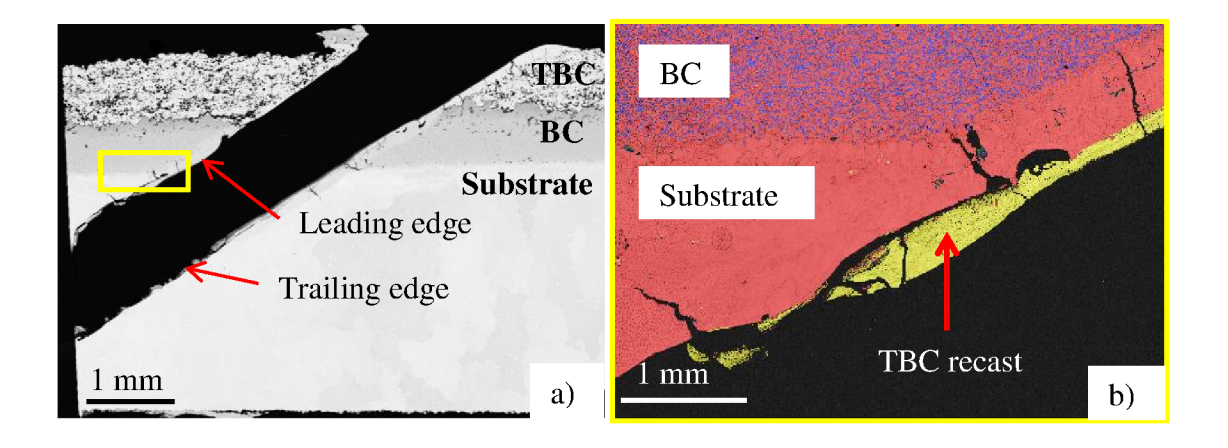


Figure 14 As-drilled specimen (BC type: aluminized LCO22), drilled by fiber laser, trepanation mode. (a) SEM image of cross-section and (b) EBSD phase map of the marked area in (a), yellow: ZrO₂, red: Ni-fcc, blue: beta-NiAl.

EBSD orientation mapping of the section in Figure 14b on the leading edge after laser drilling is shown in Figure 15. Grains in the BC/substrate recast layer are oriented mainly in the perpendicular direction to the hole wall, which makes this layer prone to crack initiation in the direction parallel to hole edge.

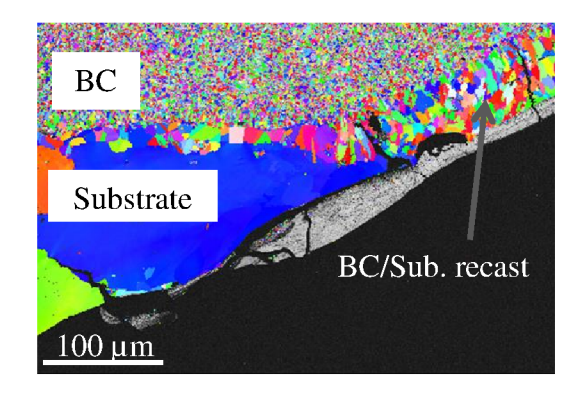


Figure 15 EBSD orientation map for specimen drilled with fiber laser, trepanation mode, at the BC/substrate interface on the leading edge, shown in Figure 14b.

In the EDS mapping of the leading edge, a larger concentration of Co can be observed in the BC/substrate recast layer, see Figure 16a, supposedly as a result of mixture of molten BC, with much larger Co content, and substrate during laser drilling, where the molten recast layer flows usually downward in the final steps of the trepanation drilling [6]. Aluminum can also be found in the TBC recast layer, see Figure 16b, which originates most likely from both BC and substrate. Based on the EDS mapping, the TBC recast consisted of mainly Zr, O, Al, Cr, Co, Ni, Ti, and Mo.

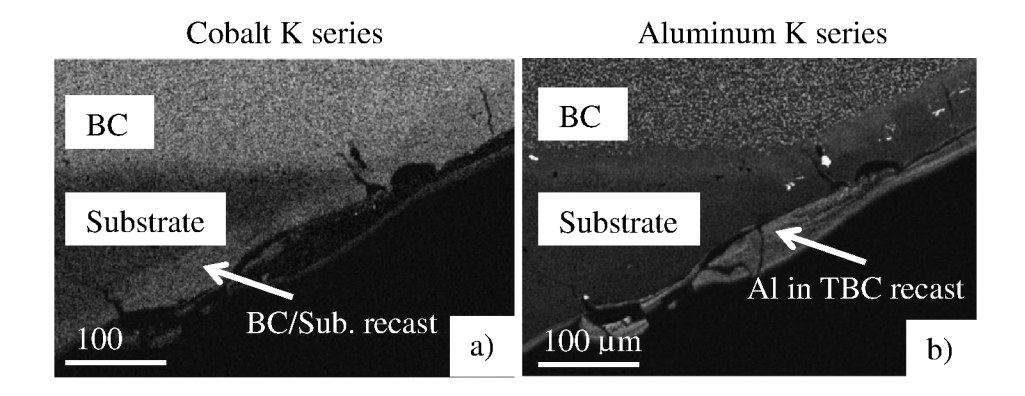


Figure 16 EDS mapping of cross-section shown in Figure 14b for a) cobalt and b) aluminum.

Microstructural analysis results of the failed specimen after cyclic oxidation, drilled with fiber laser using trepanation mode, are shown in Figure 17. It can be concluded that the delamination of TBC coating occurs mainly at the TBC/BC interface (Figure 17b), where a mixture of black and white failure can be found. Strong oxidation of BC and substrate is observed as well. TGO formation was observed at TBC/BC interface where the delamination crack has propagated through TGO and TBC, shown in green in Figure 17b. Oxidation and formation of TGO at TBC/BC interface has been reported extensively in literature to be critical for TBC life [30, 31]. Moreover, TGO (alumina) and spinel type oxide were also observed at BC/substrate on the leading edge near the hole as well as on the hole wall, as it is shown in green in Figure 17a and c, which has likely led to the shorter life time of laser-drilled TBC systems compared with the undrilled specimen. No significant difference in TGO thickness at TBC/BC interface was observed. However, a much larger depletion of β-NiAl phases in BC can be found at the hole, resulting in a weaker bond coating at this zone. Similarly the substrate is severely oxidized and eroded at the lower parts of the hole, see Figure 17a and c. Large amount of spinel type oxides including Cr, Co, and Al are observed on the hole wall, see Figure 18, that is due to very high temperature of the base alloy in the absence of film cooling, which is used in a gas turbine during operation to reduce the superalloy temperature. Such oxides has been reported to be detrimental for TBC life time, due to their lower mechanical strength [30]. The laser-induced cracks at the hole are critical which caused oxidation attack in BC and substrate.

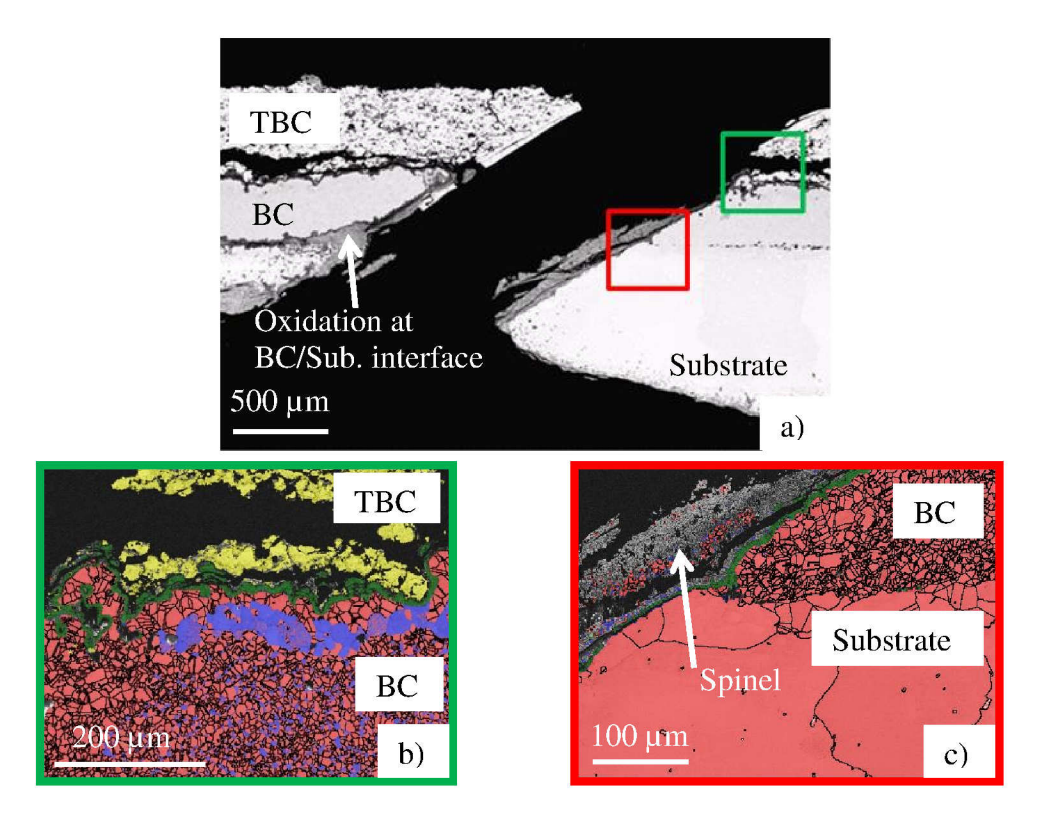


Figure 17 Microstructural images of a laser drilled specimen (BC type: aluminized LCO22) drilled by fiber laser, trepanation mode, after cyclic oxidation test; a) SEM image of the hole, b) EBSD phase map at the delamination crack near TBC/BC interface, c) EBSD phase map of the trailing edge at BC/substrate, yellow: ZrO₂, green: alumina, red: Ni-fcc, blue: beta-NiAl.

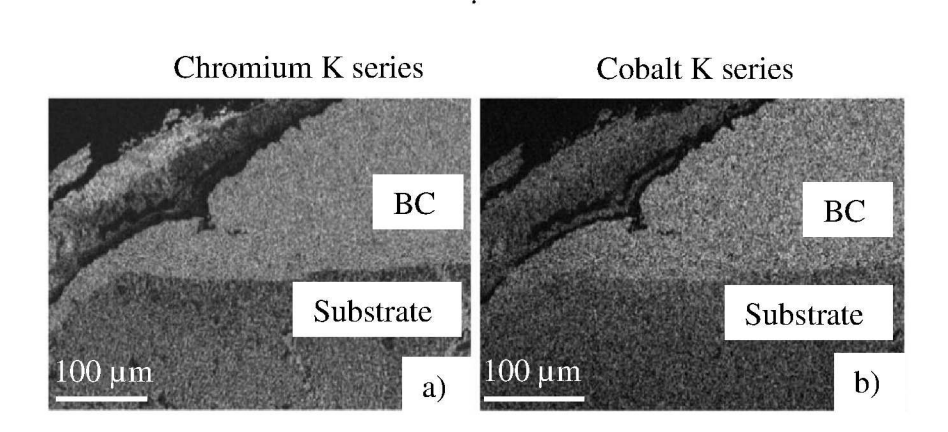


Figure 18 EDS mapping of the oxide layers on the hole wall for the cross-section shown in Figure 11c.

The oxidized areas in the BC for each specimen after failure were measured with the software AnalySIS Pro. As shown in Table 7, oxidation is stronger for specimens drilled via percussion drilling than trepanation drilling. The reason is most likely the lower quality of the hole wall due to larger crack length caused by percussion mode, as indicated by the results in Table 5.

Moreover, the specimens with inclined holes showed stronger oxidation than vertical holes, which is due to their larger defects after laser drilling.

Table 7 Comparison of crack densities at the hole wall of failed specimens.*EF: Experimental set-up failure.

Oxidation attack area (mm ² × 10 ⁻³)	Percussion	1			Trepanat	ion
BC type	LCO22		PWA286		LCO22	PWA286
Flash lamp	30° 20 ± 22.4	90° 10 ± 13	30°	90° 3.1 ± 1.2	30°	30°
Fiber laser	EF*		20 ± 25	-	7 ± 5.4	3.6 ± 6

The difference between fiber laser drilling for percussion and trepanation drilling after cyclic oxidation is represented in Figure 19. The amount of oxidation attacks in BC appears to be more critical for percussion drilling, which is probably due to low quality of the drilling process, especially the laser-induced cracks.

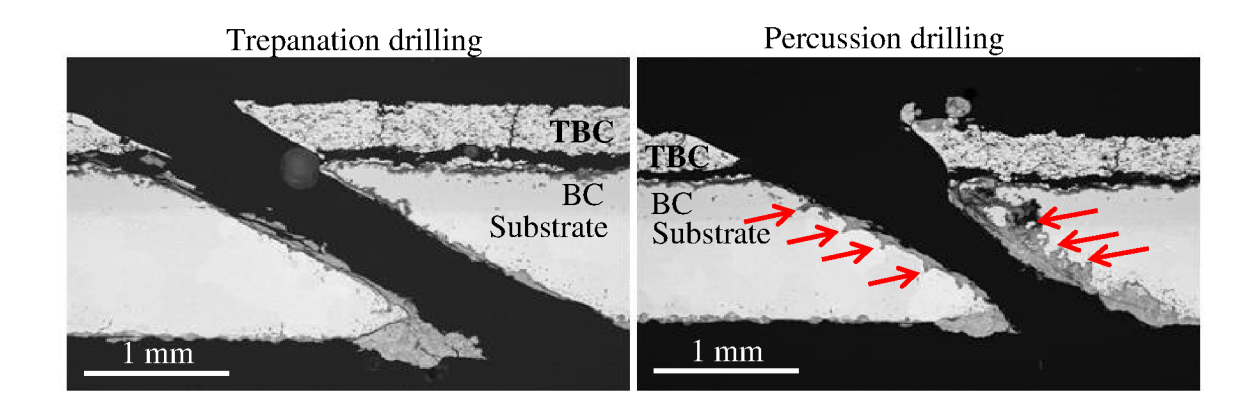


Figure 19 Comparison of specimens with PWA286 BC drilled by fiber laser using trepanation drilling (left) and percussion drilling (right).

4. Conclusion

The following conclusions can be drawn from this work:

- 1. Comparing percussion and trepanation drilling modes by fiber laser, the former caused larger cracks, which appears to be due to higher pulse energy of such drilling mode. By trepanation, the recast layer is observed to be thinner since the melt ejection is likely accelerated by vaporization of the melt due to the higher pulse intensity in this mode.
- 2. By percussion drilling, fiber laser caused lager defects at the hole compared with flash lamp laser, perhaps due to higher pulse frequency by the former laser method.
- 3. Thermography images of thermally cycled inclined holes have shown that delamination occurs at the leading edge as well as at the sidewall near it, which can be explained with higher forces during laser drilling and higher stresses due to geometry, in comparison with vertical holes. For inclined holes, delamination was more critical under cyclic oxidation in comparison with vertical holes.
- 4. Percussion and inclined drilling caused stronger oxidation in comparison with trepanation and vertical drilling, respectively, which is mainly due to the lower hole quality in these cases.

Acknowledgements

We are very thankful to the support in the Institute of Energy and Climate research (IEK-2) in Jülich by D. Liebert, J. Bartsch, V. Gutzeit, Dr. E. Wessel, Dr. D. Grüner and Prof. Singheiser, as well as D. Haasler from the Chair of Laser Technology, at RWTH Aachen University. The funding of the Ministry of Economic Affairs and Energy (BMWi) of Germany (funding number: 03ET7027C) and the support by the industrial partners, Dr. W. Stamm from Siemens AG and Dr. R. Herzog and M. Ernsberger from MAN Energy Solutions SE for this project are also immensely appreciated.

References

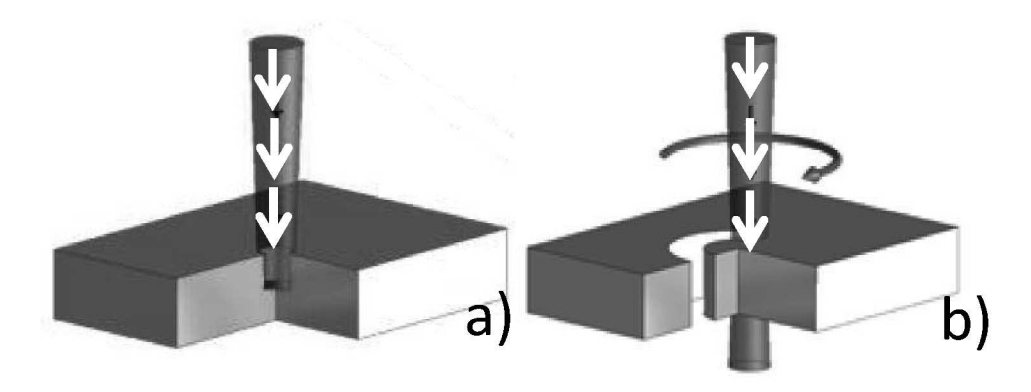
- [1] T. Isaiah, S. Dabbashi, D. Bosak, S. Sampath, G. D. Lorenzo, P. Pilidis, Life Analysis of Industrial Gas Turbines Used As a Back Up to Renewable Energy Sources, The Fourth International Conference on Through-life Engineering Services, 38 (2015) 239 244
- [2] H. Lau, U. Schulz, C. Friedrich, Influence of bondcoat pre-treatment and surface topology on the lifetime of EB-PVD TBCs, Surf. Coat. Tech., 165(3) (2003) 217 223.
- [3] D. Schwingel, R. Taylor, T. Haubold, J. Wigren, C. Gualco, Mechanical and thermophysical properties of thick PYSZ thermal barrier coatings: correlation with microstructure and spraying parameters, Surf. Coat. Tech., 108 -109 (1998) 99 -106.
- [4] D. Robb, Thermal barrier coatings and surface technologies lead the push toward greater efficiency and lower life cycle costs, Turbomach. Int., (July/August 2014) 20 22.
- [5] C. A. McNally, J. Folkes, I.R. Pashby, Laser drilling of cooling holes in aeroengines: state of the art and future challenges, Mater. Sci. Technol., 20 (2004) 805 813.
- [6] M. Antar, D. Chantzis, S. Marimuthu, P. Hayward, High Speed EDM and Laser Drilling of Aerospace Alloys, Procedia CIRP, 42 (2016) 526 531.
- [7] J.J. Klabbers-Heimann, Anwendungsgrenzen von modernen Nickelbasis- Superlegierungen in effusionsgekühlten Bauteilen zukünftiger Gasturbinen, RWTH Aachen University, 2003.
- [8] H. K. Sezer, A. J. Pinkerton, L. Li, An investigation into delamination mechanisms in inclined laser drilling of thermal barrier coated aerospace superalloys, J. Laser Appl., 17 (2005) 225 225.
- [9] H. K. Sezer, L. Li, M. Schmidt, A.J. Pinkerton, B. Anderson, P. Williams, Effect of beam angle on HAZ, recast and oxide layer characteristics in laser drilling of TBC nickel superalloys, Int. J. Mach. Tool. Manuf., (2006) 1972 1982.
- [10] G. D. Gautam, A.K. Pandey, Pulsed Nd:YAG laser beam drilling: A review, Opt. Laser. Technol., 100 (2018) 183 215.
- [11] N. I. Morar, R. Roy, J. Mehnen, S. Marithumu, S. Gray, T. Roberts, J. Nicholls, Investigation of recast and crack formation in laser trepanning drilling of CMSX-4 angled holes, Int. J. Adv. Manuf. Technol., 95 (2018) 4059 4070.
- [12] K.T. Voisey, S.S. Kudesia, W.S.O. Rodden, D.P. Hand, J.D.C. Jones, T.W. Clyne, Melt ejection during laser drilling of metals, Mater. Sci. Eng., A356 (2003) 414 424.
- [13] W.T. Chien, S.C. Hou, Investigating the recast layer formed during the laser trepan drilling of Inconel 718 using the Taguchi method, Int. J. Adv. Manuf. Technol., 33 (2007) 308 316.
- [14] C.Y. Yeo, S.C. Tam, S. Jana, M.W.S. Lau, A technical review of the laser drilling of aerospace materials, J. Mater. Process. Technol., 42 (1994) 15 49.

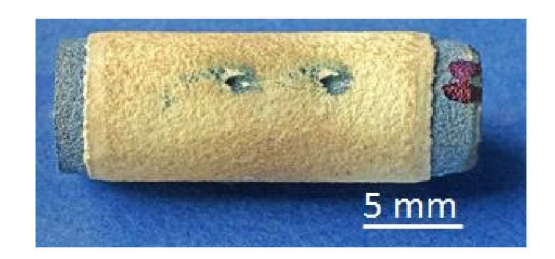
- [15] D. Ramanathan, P.A. Molian, Micro- and Sub-Micromachining of Type IIa Single Crystal Diamond Using a Ti:Sapphire Femtosecond Laser, J. Manuf. Sci. Eng., 124 (2002) 389 396
- [16] J. Kamalu, P. Byrd, A. Pitman, Variable angle laser drilling of thermal barrier coated nimonic, J. Mater. Process. Technol., 122 (2002) 355 362.
- [17] J. Girardot, M. Schneider, L. Berthe, V. Favier, Investigation of delamination mechanisms during a laser drilling on a cobalt-base superalloy, J. Mater. Process. Technol., 213 (2013) 1682 1691.
- [18] E. Lugscheider, K. Bobzin, M. Maes, K. Lackner, R. Poprawe, E. W. Kreutz, J. Willach, Laser Drilled Microholes in Zirconia Coated Surfaces using Two Variants to Implement the Effusion Cooling of First Stage Turbine Blades, Adv. Eng. Mater., 7 (2005) 145-152.
- [19] M. Tanaka, C. Mercer, Y. Kagawa, A. G. Evans, Thermomechanical Fatigue Damage Evolution in a Superalloy/Thermal Barrier System Containing a Circular Through Hole, J. Am. Ceram. Soc., 94 (2011) 128 135.
- [20] D.K. Das, T.M. Pollock, Femtosecond laser machining of cooling holes in thermal barrier coated CMSX4 superalloy, J. Mater. Process. Technol., 209 (2009) 5661 5668.
- [21] M. Schweda, T. Beck, L. Singheiser, Thermal cycling damage evolution of a thermal barrier coating and the influence of substrate creep, interface roughness and pre-oxidation, Int. J. Mater. Res., 103 (2012) 40 49.
- [22] B. Srivathsa, D.K. Das, Parametric studies of failure mechanisms in thermal barrier coatings during thermal cycling using FEM, 20 (2015) 899 915.
- [23] K. Dou, E.T. Knobbe, R.L. Parkhill, B. Irwin, L. Matthews, K.H. Church, Femtosecond study of surface structure and composition and time-resolved spectroscopy in metals, Appl. Phys. A, 76 (2003) 303 307.
- [24] Q. Feng, Y.N. Picard, J.P. McDonald, P.A. Van Rompay, S.M. Yalisove, T.M. Pollock, Femtosecond laser machining of single-crystal superalloys through thermal barrier coatings, Mater. Sci. Eng. A, 430 (2006) 203 207.
- [25] A. Neidel, S. Riesenbeck, T. Ullrich, J. Völker, C. Yao, Hot cracking in the HAZ of laser-drilled turbine blades made from René 80, Materials Testing, 47 (2005) 553-559.
- [26] M.C. Chaturvedi, Liquation Cracking in Heat Affected Zone in Ni Superalloy Welds, Materials Science Forum, 546-549 (2007) 1163-1170.
- [27] H. K. Sezer, L. Li, Mechanisms of acute angle laser drilling induced thermal barrier coating delamination, J. Manuf. Sci. Eng., 131 (2009) 051014:051011 051016.
- [28] M.E. Schweda, Optimierung von APS-ZrO₂-Wärmedämmschichten durch Variation der Kriechfestigkeit und der Grenzflächenrauhigkeit, RWTH Aachen University, 2013.
- [29] D.E. Mack, R.P. Vassen, D. Stöver, Tools for online monitoring of failure evolution of thermal barrier coatings in gas burner thermal cycling rig environment, Int. Therm. Spray. Conf., (2008) 1050 1055
- [30] O. Trunova, Effect of thermal and mechanical loadings on the degradation and failure modes of APS TBCs, RWTH Aachen University, 2006.

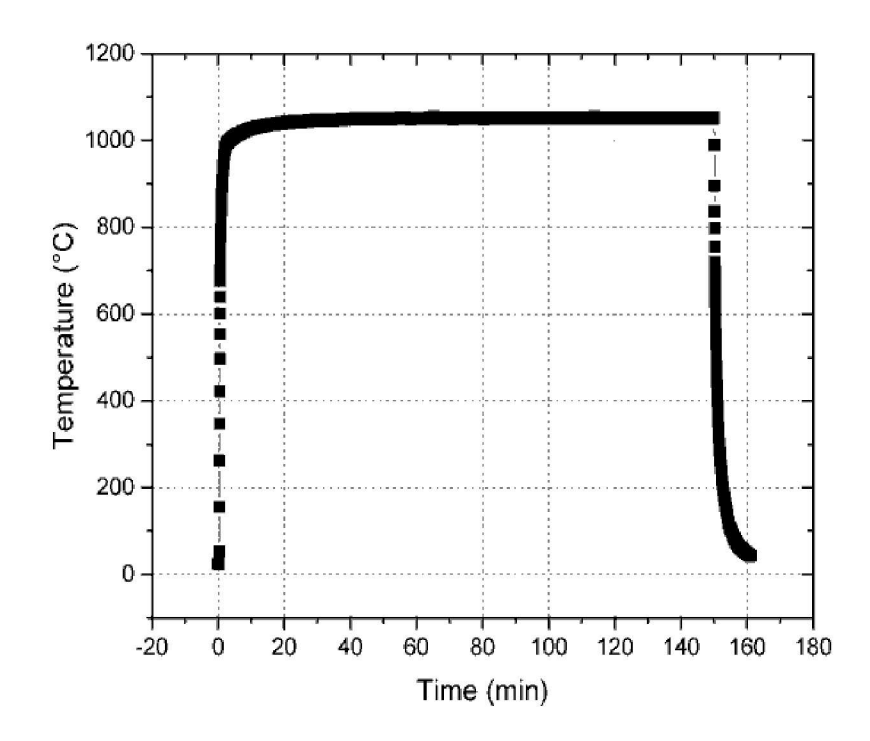
[31] T. Beck, R. Herzog, O. Trunova, M. Offermann, L.S. R.W. Steinbrech, Damage mechanisms and lifetime behavior of plasma-sprayed thermal barrier coating systems for gas turbines — Part II: Modeling, Surf. Coat. Tech., 202 (2008) 5901-5908.

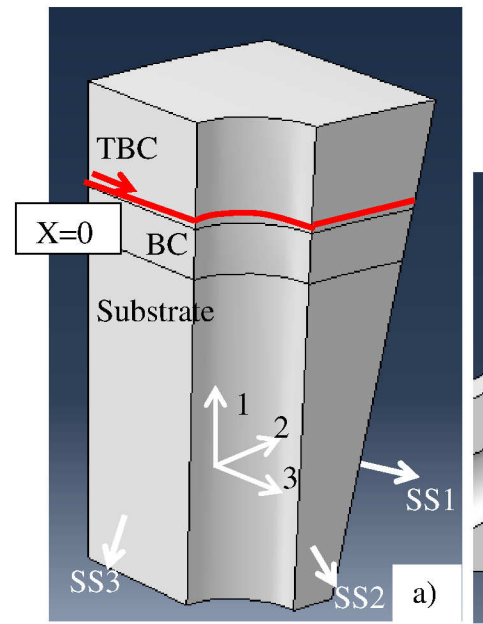
Figure 1a) Percussion and b) trepanation drilling
Figure 2 A cyclic-oxidation-specimen with laser drilled holes
Figure 3 Measured specimen's temperature in the cyclic oxidation oven
Figure 4 The red path TBC/BC interface over which the stress distributions are shown for (a)
vertical and (b) inclined cooling hole
Figure 5 SEM images of specimens drilled with fiber laser using trepanation mode for a) 90° and
b) 30° holes, and percussion mode similarly for a c) 90° and d) 30° holes. Arrows in red show
cracks at TBC/BC interface, and arrows in white indicate cracks in TBC recast layer 11
Figure 6 a) A TBC system drilled by a ms-pulsed laser with b) TBC and c) substrate/BC recast
layer
Figure 7 SEM images of specimens drilled with a) ultra-short pulsed laser, and magnified image
b) at TBC/BC interface, and c) at BC/substrate image
Figure 8 The TBC undercutting observed for the case of a) fiber laser, percussion, compared with
b) flash lamp, percussion laser drilling
Figure 9 Comparison of BC/Sub. recast thickness and crack length for a) fiber laser, trep., 30°, b)
fiber laser, trep., 90° , c) fiber laser, perc., 30° , d) fiber laser, perc., 90° , e) flash laser, perc., 30° , f)
flash laser, perc., 90°
Figure 10 The development of delamination for specimens during cyclic oxidation test, drilled by
flash lamp laser, with a) 30° and b) 90° cooling holes
Figure 11 The development of delamination for the laser drilled specimen due to cyclic oxidation.
Type 1: specimens with aluminized LCO22 as BC, and type 2: specimens with PWA286 BC 18
Figure 12 Schematic presentation of an inclined hole with the critical position at the TBC/BC
interface for crack initiation and propagation under a cyclic oxidation loading condition 18
Figure 13 Stress distribution in the normal direction 1 at TBC/BC interface for a) vertical and b)
inclined hole, c) normal stress profile at TBC/BC interface for both angles

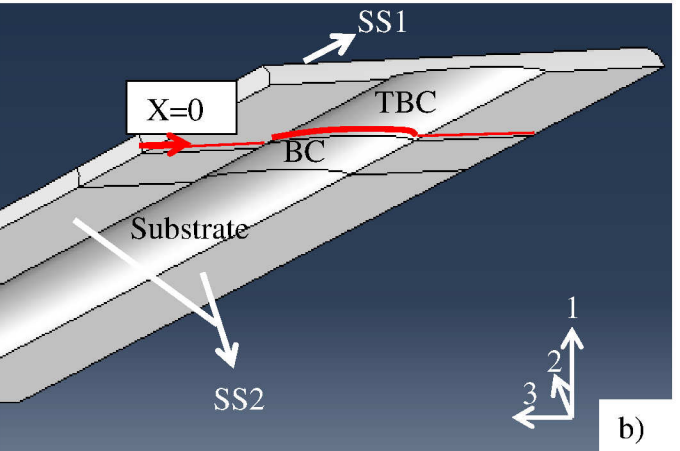
Figure 14 As-drilled specimen (BC type: aluminized LCO22), drilled by fiber laser, trepanation
mode. (a) SEM image of cross-section and (b) EBSD phase map of the marked area in (a), yellow:
ZrO ₂ , red: Ni-fcc, blue: beta-NiAl. 20
Figure 15 EBSD orientation map for specimen drilled with fiber laser, trepanation mode, at the
BC/substrate interface on the leading edge, shown in Figure 14b
Figure 16 EDS mapping of cross-section shown in Figure 14b for a) cobalt and b) aluminum 21
Figure 17 Microstructural images of a laser drilled specimen (BC type: aluminized LCO22)
drilled by fiber laser, trepanation mode, after cyclic oxidation test; a) SEM image of the hole, b)
EBSD phase map at the delamination crack near TBC/BC interface, c) EBSD phase map of the
trailing edge at BC/substrate, yellow: ZrO ₂ , green: alumina, red: Ni-fcc, blue: beta-NiAl 23
Figure 18 EDS mapping of the oxide layers on the hole wall for the cross-section shown in Figure
11c
Figure 19 Comparison of specimens with PWA286 BC drilled by fiber laser using trepanation
drilling (left) and percussion drilling (right).

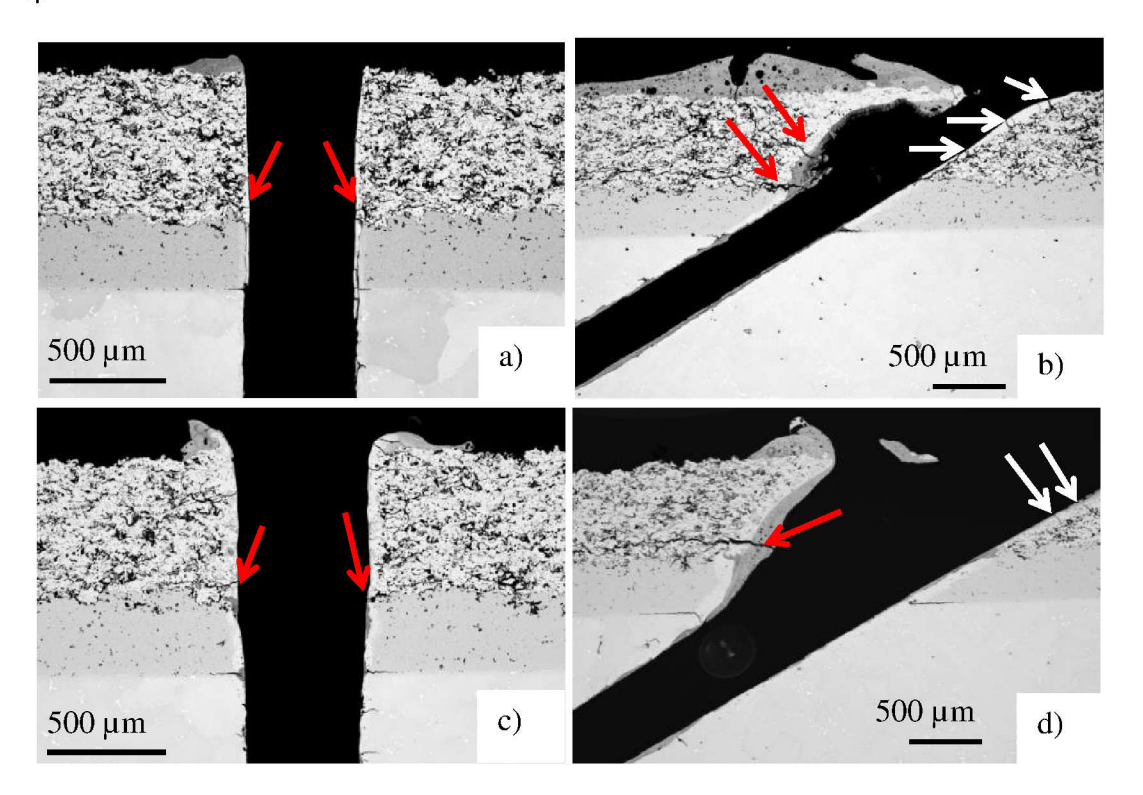


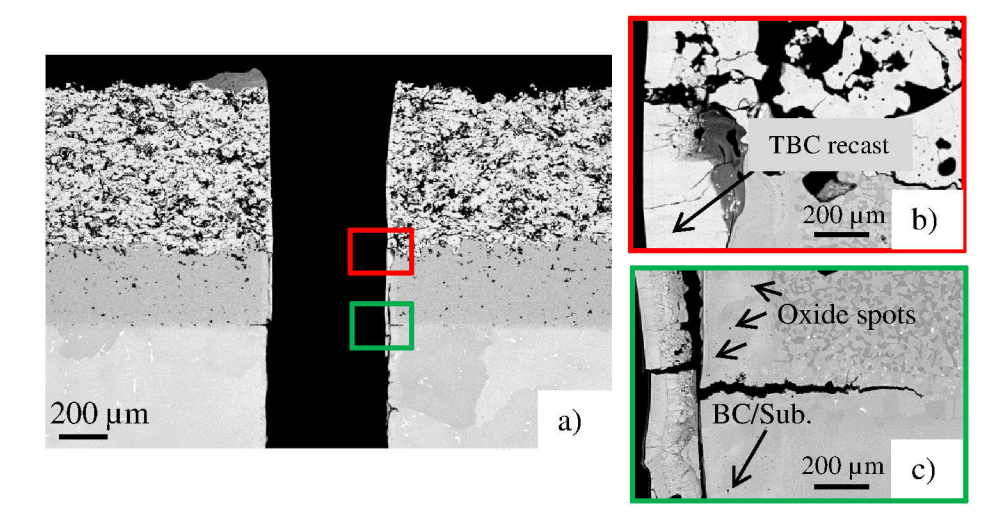


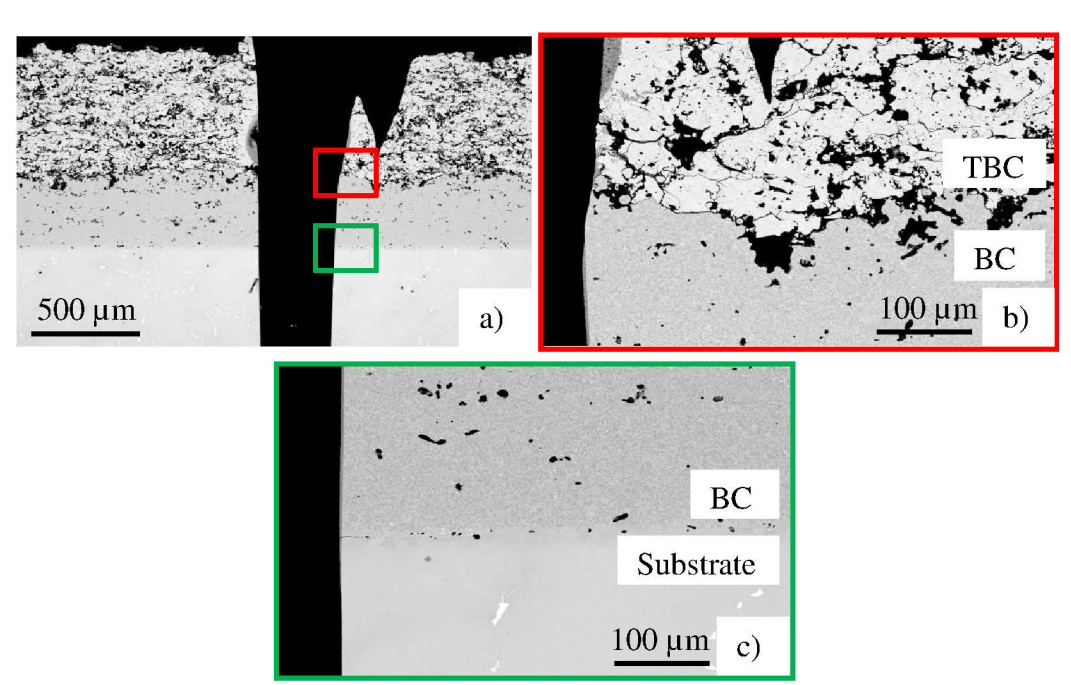


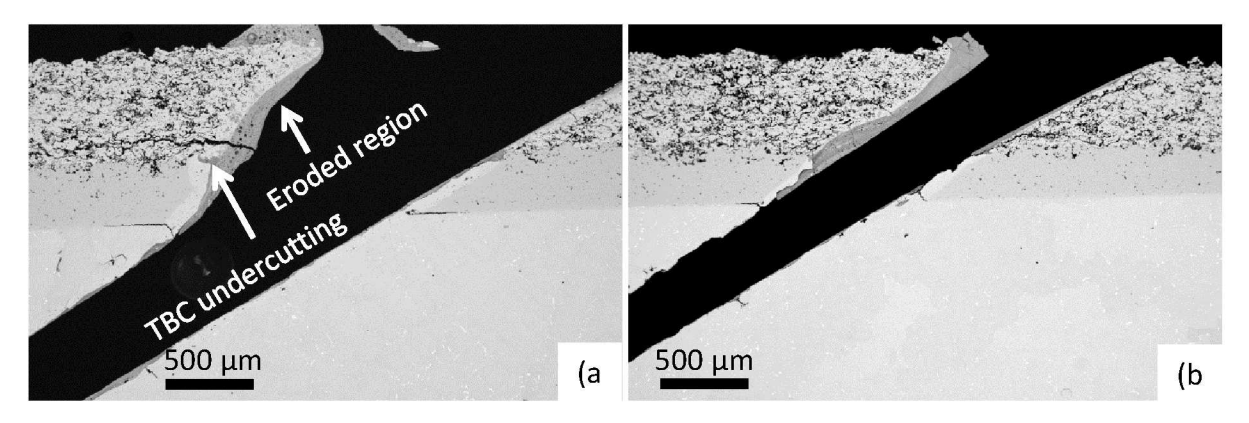


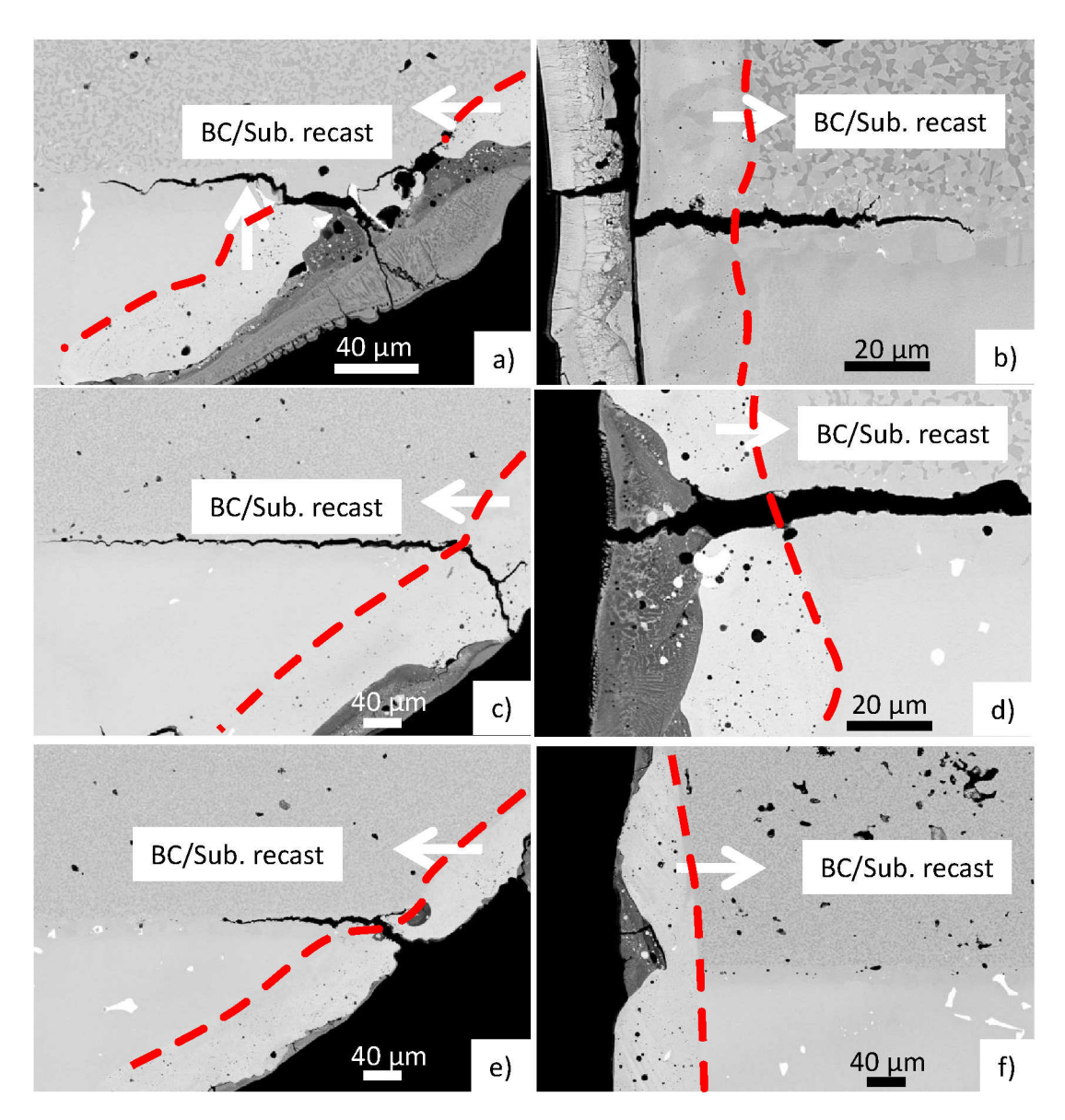


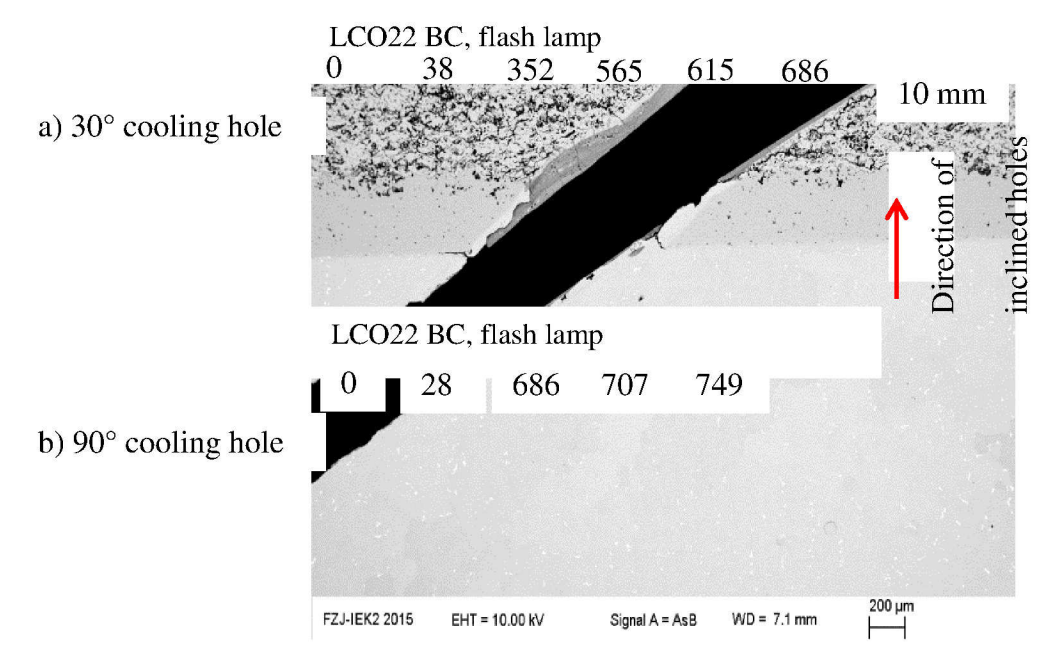


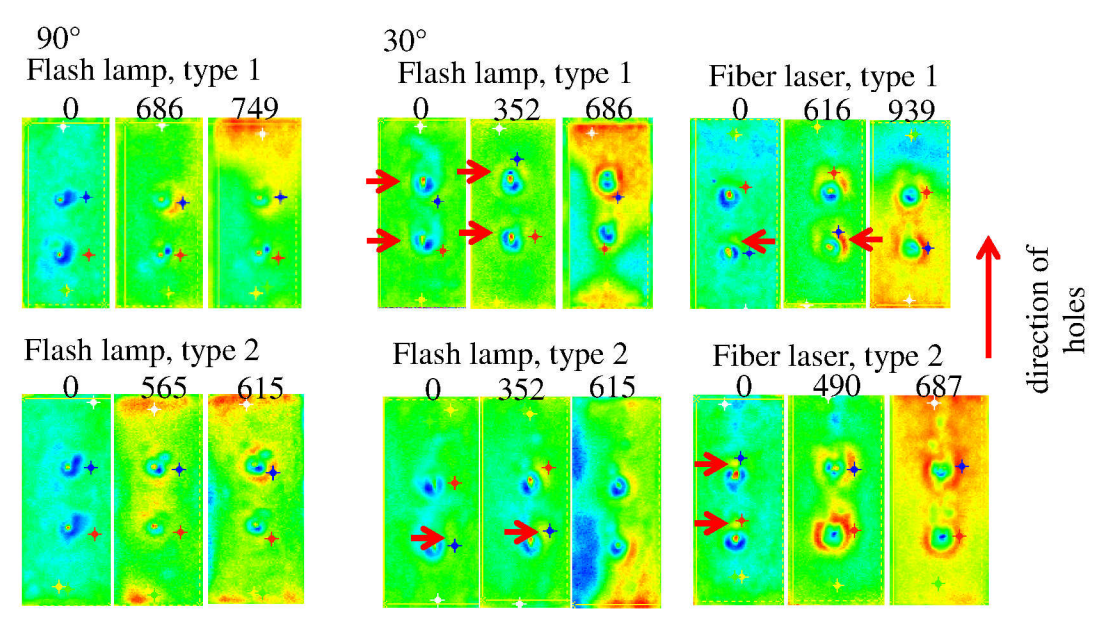


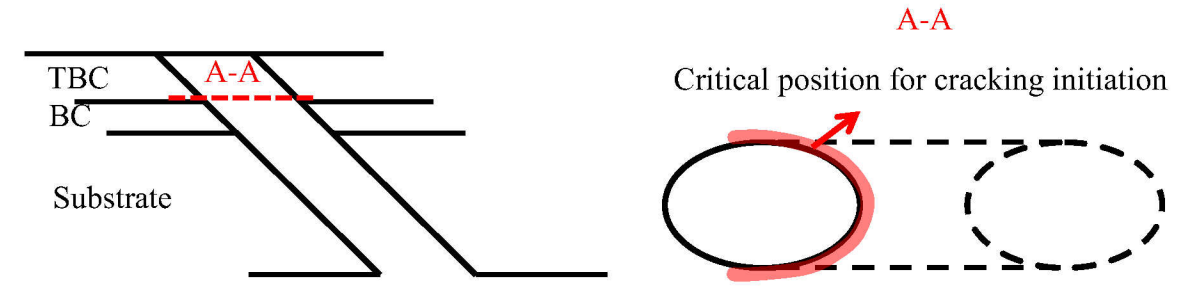


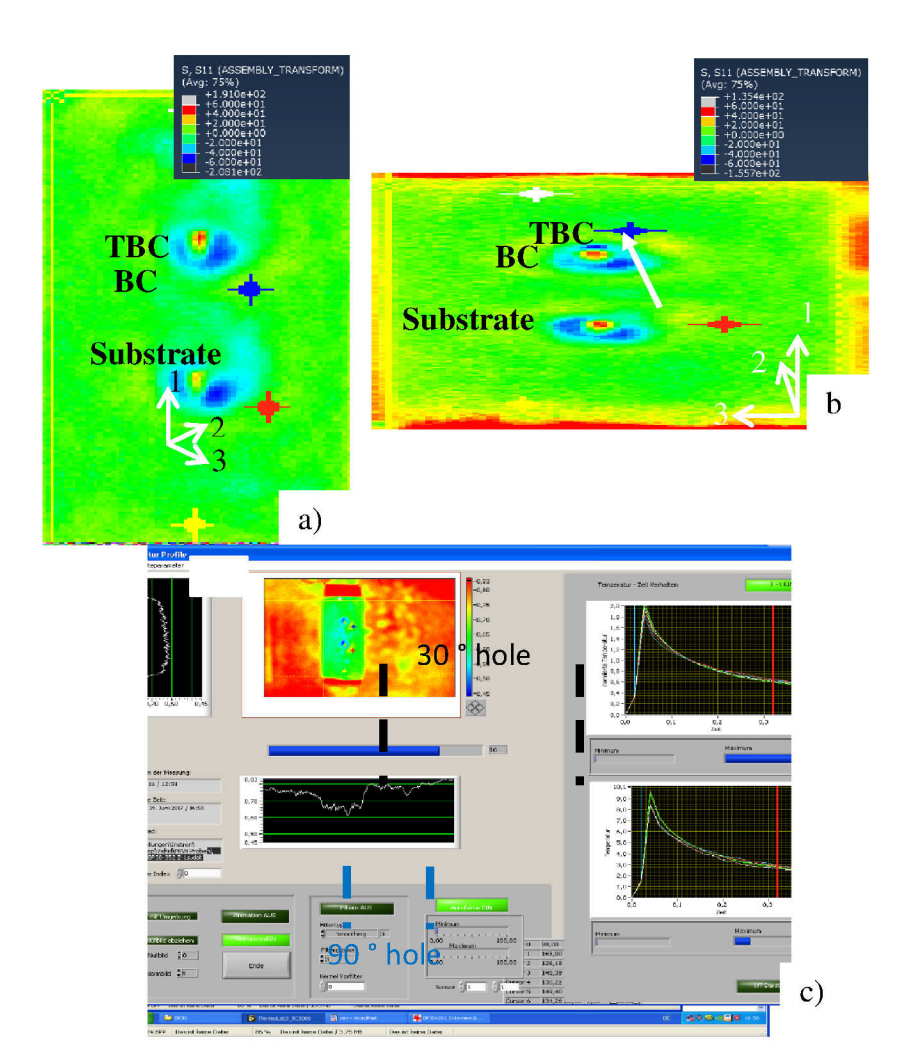


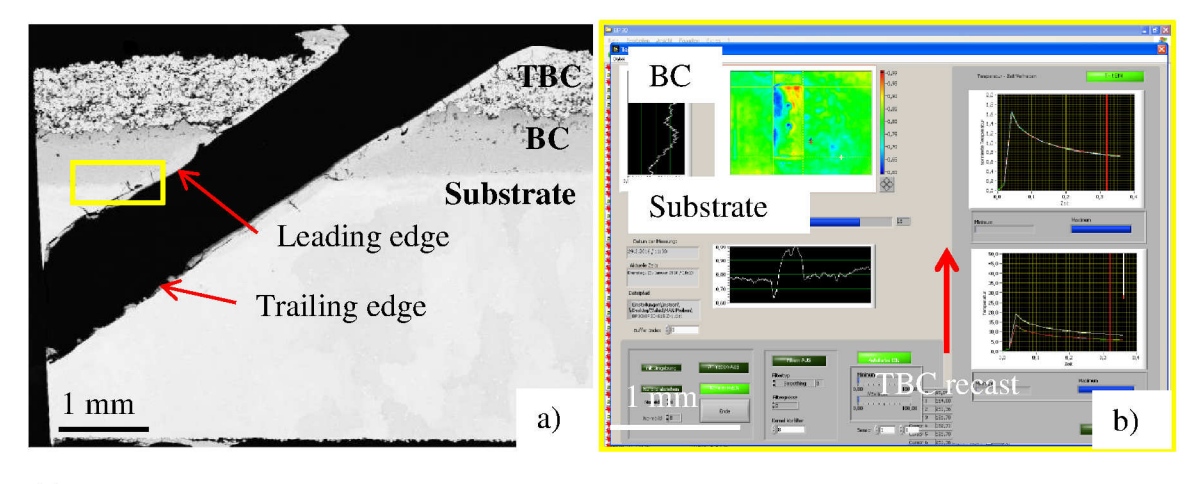


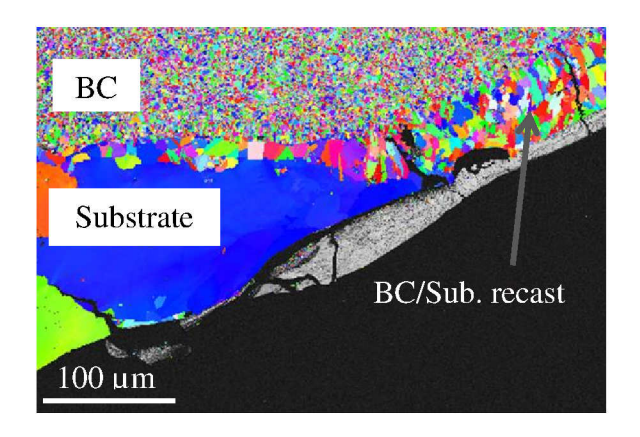










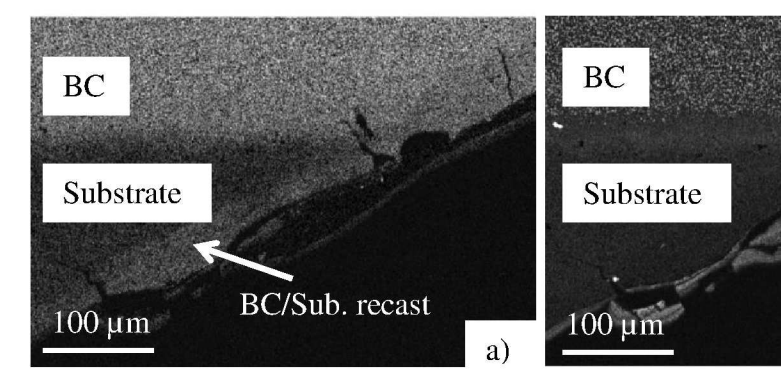


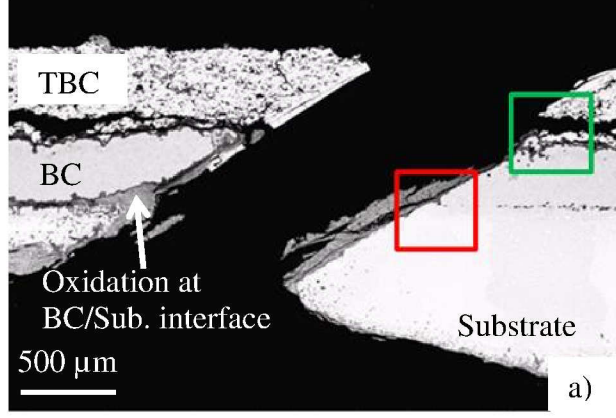
Cobalt K series

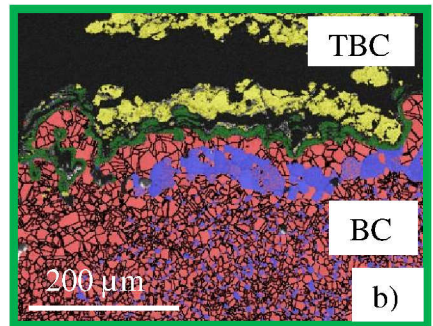
Aluminum K series

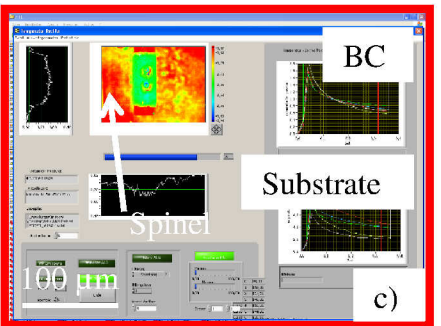
Al in TBC recast

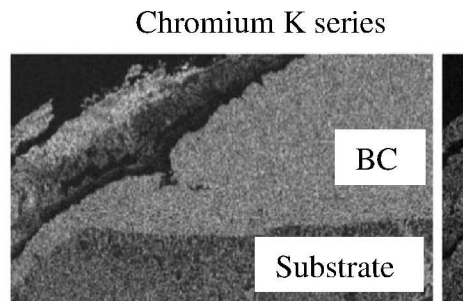
b)

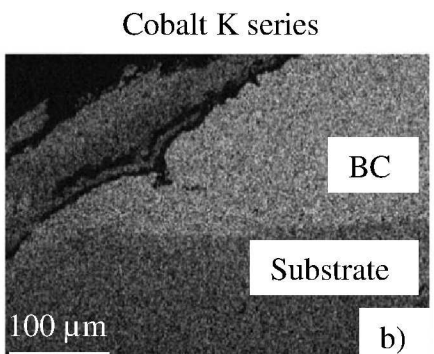




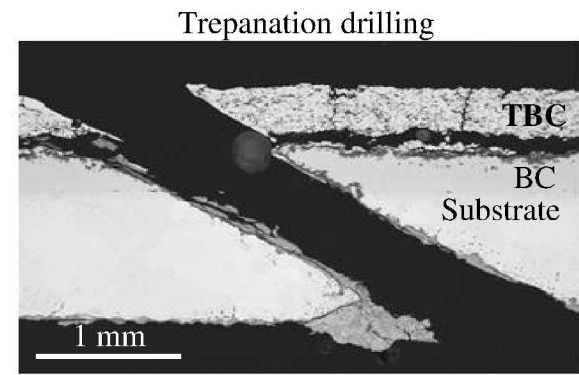








 $100 \; \mu m$



a)

